ORGANOMETALLICS

pubs.acs.org/Organometallics Article

Computational Investigations of Enantioselection in Carbon— Carbon Bond Forming Reactions of Ruthenium Guanidinobenzimidazole Second Coordination Sphere Hydrogen Bond Donor Catalysts

Taveechai Wititsuwannakul, Tathagata Mukherjee, Michael B. Hall,* and John A. Gladysz*



Cite This: *Organometallics* 2020, 39, 1149–1162



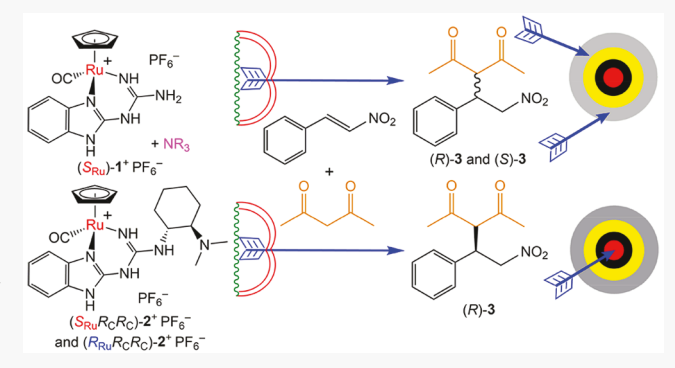
ACCESS

III Metrics & More

Article Recommendations

s Supporting Information

ABSTRACT: The NH₂ group of 2-guanidinobenzimidazole (GBI) can be replaced by (R_CR_C) -NHCH(CH₂)₄CHNMe₂ and elaborated to the enantiopure chelate salts $(S_{Ru}R_CR_C)$ - $[(\eta^5-C_5H_5)Ru(CO)(GBICH(CH_2)_4CHNMe_2)]^+PF_6^-$ ($(S_{Ru}R_CR_C)$ - $2^+PF_6^-$) and $(R_{Ru}R_CR_C)$ - $2^+PF_6^-$. These catalyze highly enantioselective additions of 1,3-dicarbonyl compounds to nitroalkenes. The mechanism and basis for enantioselection are probed by DFT calculations. First, the parent GBI complex $[(\eta^5-C_5H_5)Ru(CO)-(GBI)]^+PF_6^-$ ($(1^+PF_6^-)$ is examined. This species has only ruthenium-centered chirality and must be used with a trialkylamine, as it lacks the internal base of $(2^+PF_6^-)$. The dicarbonyl compound initially hydrogen bonds to the NH triad of the GBI



ligand, but the transition states leading to each product enantiomer are essentially equal in energy. In contrast, after similar bonding of the dicarbonyl compound to $(S_{Ru}R_CR_C)$ - or $(R_{Ru}R_CR_C)$ -2+PF₆⁻, a proton is transferred to the :NMe₂ moiety, giving an enolate and a HNMe₂⁺ group. The latter mediates the introduction of *trans-\beta*-nitrostyrene such that one enolate π face attacks the C_{si} = C_{re} Ph face to give an addition product with an R configuration, in agreement with experiment. Thus, the configurations of the catalyst carbon stereocenters control the product stereochemistry. Interactions in competing transition states are analyzed.

■ INTRODUCTION

There is an extensive literature of chiral "organocatalysts" that serve as hydrogen bond donors and effect a variety of organic reactions with high enantioselectivities. Over the past few years, we have sought to develop complementary metal-containing chiral hydrogen bond donors, as metal complexes exhibit diverse types of chirality motifs, many of which have proved to be highly successful for other types of enantioselective catalysis. Our efforts have focused on NH donor groups, either directly coordinated or remote from the metal, as exemplified in Figure 1. Related themes have been explored by other research groups.

In many of these reactions, enantioselectivities have routinely exceeded 90% ee. 4b-e,g,5b However, there is the potential for enhanced mechanistic complexity, as most nitrogenous organic hydrogen bond donor catalysts feature 2 NH groups (e.g., N,N'-diaryl thioureas), whereas the systems in Figure 1 possess 4–12. Although it seems unlikely that the organic substrates would interact with more than 4–5 NH groups in any transition state assembly, a plethora of possibilities nevertheless remain. Hence, it has not been

possible to formulate transition state models that would help to rationally optimize this chemistry.

Accordingly, in this paper we focus on one of the most successful types of catalysts, the bifunctional ruthenium systems ($S_{Ru}R_CR_C$)- and ($R_{Ru}R_CR_C$)- $2^+PF_6^-$ (Figure 1, bottom), which contain both ruthenium and carbon stereocenters as well as a pendant tertiary amine. As shown in Scheme 1, these effect highly enantioselective Michael additions of malonate esters to $trans-\beta$ -nitroalkenes. The monofunctional ruthenium complex $1^+PF_6^-$ and the related salts $1'^+X^-$ (Figure 2, middle) can also, in conjunction with the external tertiary amine NEt3, serve as catalysts, but it has not yet proved possible to isolate these species in enantiomerically pure form.

Received: February 3, 2020 Published: April 14, 2020





Figure 1. Some previously studied metal-containing chiral hydrogen bond donor catalysts.

Scheme 1. Additions of Diethyl Malonate to Nitroalkenes Catalyzed by $(S_{Ru}R_CR_C)$ - and $(R_{Ru}R_CR_C)$ -2⁺PF₆⁻

$\begin{array}{c ccccccccccccccccccccccccccccccccccc$				
R	(<i>S</i> _{Ru} <i>R</i> _C <i>R</i> _C yield (%)		(R _{Ru} R _C R _C) yield (%)	
	95 ^a	93 ^a	92 ^a	91 ^a
CI	>99	93	96	96
Co	85	>99	74	>99
174-	49	83	41	87

^aData for the analogous reaction of dimethylmalonate: 97%, 91%, 95%, 88%

In this paper, we present an extended series of DFT calculations that establish the most probable modes of substrate binding to $\mathbf{1}^+\mathrm{PF}_6^-$, $(S_{\mathrm{Ru}}R_{\mathrm{C}}R_{\mathrm{C}})\mathbf{-2}^+\mathrm{PF}_6^-$, and $(R_{\mathrm{Ru}}R_{\mathrm{C}}R_{\mathrm{C}})\mathbf{-2}^+\mathrm{PF}_6^-$, as well as transition state assemblies that are in accord with the dominant product configurations obtained with $\mathbf{2}^+\mathrm{PF}_6^-$. Transition state assemblies derived from $\mathbf{1}^+\mathrm{PF}_6^-$ are also examined, but using NMe₃ in place of NEt₃ to

simplify the computations. These help to define the effect of the added carbon stereocenters and functionality in $2^+PF_6^-$ upon enantioselectivities, an objective that is not yet addressable experimentally.

EXPERIMENTAL SECTION

Reaction in Scheme 2. A J. Young NMR tube was charged with 2,4-pentanedione (0.0184 g, 0.200 mmol), $trans-\beta$ -nitrostyrene (0.0298 g, 0.200 mmol), and CD_2Cl_2 (1.0 mL). Then $(S_{Ru}R_CR_C)$ or $(R_{Ru}R_{C}R_{C})-2^{+}PF_{6}^{-}$ (0.0013 g, 0.0020 mmol, 1.0 mol %)^{5b} was added. The sample was capped and monitored by NMR and TLC. After 24 h, the solvent was removed. The residue was taken up in hexane/ethyl acetate (30/70 v/v). The sample was passed through a short silica gel column, which was washed with additional hexane/ ethyl acetate (50/50 v/v, 5 mL). The solvent was removed from the combined eluate, and a second silica gel chromatography step was carried out. The solvent was removed from the product-containing fractions to give the previously reported 3-(2-nitro-1-phenylethyl)-pentane-2,4-dione (3) as colorless needles (from $(S_{Ru}R_{C}R_{C})-2^{+}PF_{6}^{-}$, 0.0349 g, 0.140 mmol, 70%; from $(R_{Ru}R_{C}R_{C})-2^{+}PF_{6}^{-}$, 0.0374 g, 0.150 mmol, 75%). NMR $(\delta, CDCl_{3})$: 8,9 ^{1}H (500 MHz) 7.34–7.25 (m, 3H), 7.19-7.16 (m, 2H), 4.64-4.61 (m, 2 H), 4.36 (d, 1H, J = 10.7 Hz), 4.27-4.20 (m, 1H), 2.28 (s, 3H), 1.93 (s, 3H); ¹³C{¹H} (125 MHz) 201.6, 200.9, 135.9, 129.3, 128.5, 127.9, 78.2, 70.7, 42.9, 30.5, 29.7 (11 \times s). The enantiomeric excess was determined by HPLC with a Chiralpak AS-H column, hexane/2-PrOH (85/15 v/v), 1.0 mL/min, $\lambda = 215$ nm; $t_R = 14.9$ min (minor, S), 22.6 min (major, $R).^{10}$

General procedures and instrumentation were identical with those given in a previous paper. 5b 2,4-Pentanedione was used as received from Aldrich (99%).

Computational Details. All calculations were performed with the Gaussian 09 program, revision D.01. A wide variety of alternative structures for intermediates and transition states was explored with numerous arrangements of the substrates and catalysts as well as hydrogen bond interactions. The structures were initially optimized in the gas phase with the ω B97X-D functional (range-separated hybrid generalized gradient approximation RSH-GGA). 12 This functional has been successfully used to study other reactions involving ruthenium catalysts¹³ and was similarly employed for geometry optimizations and frequency calculations in this work with basis set 1 (BS1). BS1 consists of the Stuttgart relativistic small core (RSC) 1997 ECP basis set 14 for ruthenium atoms and the 6-31G(d,p) basis set 15 for other atoms. Solution-phase optimization was important here, as the dipole moments are large and sensitive to the gas-phase and solution-phase structures (see sections S6 and S7 in the Supporting Information). Therefore, all structures were fully optimized in CH₂Cl₂ solvent (per Schemes 1 and 2) using a solvation model based on electron density (SMD; $\varepsilon = 8.93$). Frequency calculations were performed to determine free energy corrections (298.15 K) and verify the nature of (1) stationary points of intermediates with no imaginary frequency and (2) transition states with one imaginary frequency.

The ωB97X-D functional with basis set 2 (BS2) was used for single-point energy calculations on the solution-phase optimized structures. BS2 treats ruthenium analogously to BS1 and uses the 6-311++G(d,p) basis set ¹⁵ for other atoms. All energies throughout this work refer to the relative Gibbs free energies in CH₂Cl₂ calculated by ωB97X-D/BS2(SMD)//ωB97X-D/BS1(SMD). The conductor-like polarizable continuum model (CPCM)¹⁷ with UFF atomic radii was carried out as single-point calculations on the SMD solution-phase optimized structures. All Gibbs free energies in CH₂Cl₂ obtained by the SMD solvation model parallel those of the CPCM solvation model (see details in the Supporting Information). Standard conditions were corrected to 1.0 mol/L. Additional calculations were also performed with the large TZVP basis set ¹⁹ and free energy corrections with Truhlar's quasiharmonic approximation (see details in the Supporting Information). The JIMP2 molecular visualizing and manipulating program was used for all 3D molecular structures.

Figure 2. Relative free energy profiles ($\Delta G(CH_2Cl_2)$, kcal/mol) for adducts of (S_{Ru})-1⁺. Selected distances (Å): **2-I**, H_3-O_1 1.93, H_4-O_1 2.01, H_4-O_2 2.82, H_5-O_2 1.80; **2-II**, H_3-O_1 2.25, H_4-O_1 2.68, H_4-O_2 2.08, H_5-O_2 2.02, H_6-O_1 1.00, H_6-O_2 1.64; **2-III**, H_3-O_1 2.93, H_4-O_1 1.91, H_5-O_2 1.93; **2-IV**, H_3-O_1 2.70, H_4-O_1 1.89, H_5-O_2 1.96.

RESULTS

Enantioselective Catalysis: Additional Experimental Data. In exploratory DFT calculations, various ruthenium-catalyzed additions of dialkyl malonates to trans-β-nitrostyrene were investigated (see *inter alia* Scheme 1). However, the degrees of freedom associated with the alkoxy groups, which can adopt s-cis (Z) or s-trans (E) RO-C(=O) conformations, complicated the computations and analyses. Thus, the possibility of removing this variable by studying additions of a related 1,3-diketone, 2,4-pentanedione, was considered.

As shown in Scheme 2, analogous reactions of 2,4-pentanedione and $trans-\beta$ -nitrostyrene were conducted, but

Scheme 2. Additions of 2,4-Pentanedione to trans- β -Nitrostyrene Catalyzed by $(S_{Ru}R_{C}R_{C})$ - and $(R_{Ru}R_{C}R_{C})$ - $2^{+}PF_{6}^{-}$

catalyst: $(S_{Ru}R_CR_C)-2^+$ PF₆⁻, 70% yield, >99% ee $(R_{Ru}R_CR_C)-2^+$ PF₆⁻, 75% yield, >99% ee

with reduced loadings of the diastereomeric catalysts $2^+PF_6^-$ (1.0 mol % vs 10 mol %, made possible by the faster additions). Workups gave 3-(2-nitro-1-phenylethyl)pentane-2,4-dione (3), which had previously been prepared in nonracemic form,⁸ in 70–75% yields. In both cases, chiral HPLC indicated the formation of (R)-3 in >99% ee. Thus, as seen earlier in Scheme 1, the product configuration is controlled by the carbon configurations of the catalyst; the ruthenium configuration has virtually no influence.

The relative (and absolute) configurations of the *trans-β*-nitrostyrene addition products in Schemes 1 and 2 were identical. Accordingly, it was presumed that the mechanism computed for Scheme 2 would share many features with those operative in Scheme 1.

(\$\mathbb{G}_{Ru}\$)-1+: Binding of Educts. Efforts were first directed at the simpler monofunctional catalyst 1+PF₆-. In a previous paper, it was established that the PF₆- anion does not appreciably associate with the cation 1+ in CH₂Cl₂. Hence, the anion was omitted in all computations. As noted in the Experimental Section, all energies correspond to those expected in CH₂Cl₂ solution.

As depicted in Figure 2, two low-energy 1:1 adducts derived from (S_{R_1}) -1⁺ and 2,4-pentanedione were found. In the more stable adduct, 2-I, the middle NH group of the triad (N_3-H_4) binds to both dione oxygen atoms (O₁, O₂; H₄···O₁ and H₄··· O2, 2.01 and 2.82 Å), and the terminal NH groups of the triad (N_2-H_3, N_5-H_5) each bind to a single oxygen atom $(H_3\cdots O_1)$ and H₅···O₂, 1.93 and 1.80 Å). In the less stable adduct, 2-II, tautomerization has occurred to give a cyclic enol ligand. Experimentally, the free cyclic enol is slightly more stable than 2,4-pentanedione in CH_2Cl_2 (K([enol]/[dione]) = 4.2 at 20 °C; 23,24 see section S5 in the Supporting Information for similar computational results). The middle NH group of the triad exhibits hydrogen bonding similar to that of 2-I (H₄···O₂ and H₄···O₁, 2.08 and 2.68 Å), but the hydrogen bonds involving the terminal NH groups are longer and presumably weaker $(H_3 \cdots O_1 \text{ and } H_5 \cdots O_2, 2.25 \text{ and } 2.02 \text{ Å}).$

Similarly, two lower energy 1:1 adducts of (S_{R_n}) -1⁺ and *trans-\beta*-nitrostyrene were also found, **2-III** and **2-IV** (Figure 2). In both, one of the NO₂ oxygen atoms is hydrogen-bonded to two NH groups (N2-H3, N3-H4), and the other to one group (N_5-H_5) . They differ mainly in the conformation about the O_2N -CH=CHPh linkage (torsion angles differing by ca. 180°). The π faces of the CH=CHPh moiety are diastereotopic (or enantiotopic in the free ligand). That projecting toward the reader in 2-III can be designated C_{re} C_{si} Ph and that in 2-IV C_{si} = C_{re} Ph (see also Scheme 2). The average NH···O distances in the adducts are quite close (2.26 and 2.18 Å), consistent with the negligible energy difference (3.2 and 3.1 kcal/mol). When trans- β -nitrostyrene is titrated into a CD₂Cl₂ solution of racemic 1⁺BAr_f⁻, the corresponding NH ¹H NMR signals shift downfield, ^{5a} consistent with the generation of equilibrium quantities of such species. Nonetheless, binding 2,4-pentanedione to (S_{Ru}) -1⁺ remains ca. 3.4 kcal/ mol more favorable.

 (S_{Ru}) -1*: Enolate Generation. The generation of a free or coordinated enolate was presumed to be a prerequisite for carbon—carbon bond formation. The free energies of proton transfer from 2,4-pentanedione to either a NH or NH₂ group of (S_{Ru}) -1* were found to be 55.7—80.7 kcal/mol (Figure s1 in the Supporting Information), which would be prohibitive under the conditions of Scheme 1 or 2. Alternatively, the free energy of proton transfer to NMe₃ was computed to be 21.4 kcal/mol. However, the initial formation of the adducts 2-III and 2-IV in Figure 2 would add another 3 kcal/mol to this pathway.

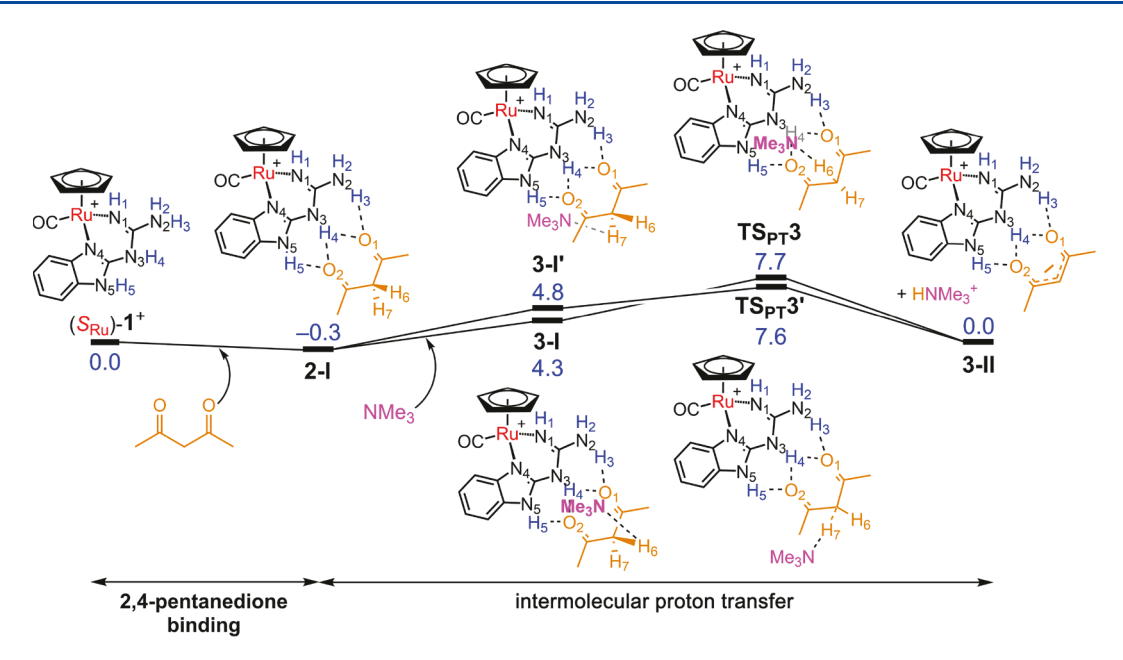


Figure 3. Relative free energy profiles ($\Delta G(CH_2Cl_2)$, kcal/mol) for 2,4-pentanedione binding to (S_{Ru})-1⁺ and subsequent intermolecular proton transfer. Selected distances (Å): 3-I, H₃-O₁ 1.87, H₄-O₁ 2.12, H₄-O₂ 2.30, H₅-O₂ 1.82, C-H₆ 1.11, H₆-N 2.20; 3-I', H₃-O₁ 1.88, H₄-O₁ 2.10, H₄-O₂ 2.19, H₅-O₂ 1.81, C-H₇ 1.12, H₇-N 2.11; TS_{PT}3, H₃-O₁ 1.81, H₄-O₁ 2.01, H₄-O₂ 2.26, H₅-O₂ 1.73, C-H₆ 1.32, H₆-N 1.41; TS_{PT}3', H₃-O₁ 1.82, H₄-O₁ 2.00, H₄-O₂ 2.33, H₅-O₂ 1.72, C-H₇ 1.31, H₇-N 1.41; 3-II, H₃-O₁ 1.70, H₄-O₁ 1.92, H₄-O₂ 2.26, H₅-O₂ 1.60.

Thus, the free energy of proton transfer from the adduct 2-I (Figure 2) to NMe₃ was examined. As shown in Figure 3, the nitrogen lone pair initially hydrogen bonds to the CH₂ moiety of the dione, via either the hydrogen atom that can be viewed as *syn* to the cyclopentadienyl ligand (3-I) or that which is *anti* (3-I'). These structures are close in energy and are only 4.3–4.8 kcal/mol above the energies of the educts. Proton transfer transition states (TS_{PT}3, TS_{PT}3') with modest 8.0–7.9 kcal/mol barriers (–0.3 vs 7.7–7.6 kcal/mol) then lead to the neutral ylide 3-II and the protonated amine HNMe₃⁺. The overall free energy change (0.0 kcal/mol) is much lower than those for the other proton transfer processes considered above. Although it is known that calculated proton transfer energies can have significant errors, ²⁵ these energies do not contribute to the reaction rate.

The N-H···O hydrogen bonds of 3-II are much shorter than those in the precursor 2-I (average: 1.87 vs 2.14 Å), reflecting the greater hydrogen bond acceptor strength that would be expected for any conjugate base. Numerous computational experiments were carried out with the enol adduct 2-II (Figure 2), but no low-lying transition states for deprotonation could be located.

(S_{Ru})-1*: Carbon–Carbon Bond Forming Step. Interactions of 3-II and trans- β -nitrostyrene were probed next. For orientation purposes, four limiting outcomes are diagrammed in Figure 4. The GBI/enolate assembly is roughly planar, and one face can be viewed as syn to the cyclopentadienyl ligand and the other anti. The nitrostyrene ligand can in principle add from both directions, using either enantioface (C_{si} = C_{re} Ph or C_{re} = C_{si} Ph). Two approaches lead to the addition product (R)-3 and the other two to (S)-3. These may be mediated by attractive noncovalent π/π interactions, NH···O hydrogen bonds, or other means.

In Figure 5, the *syn* approach of *trans-\beta*-nitrostyrene to 3-II is examined. Two lower lying adducts, 5-I and 5-I', are found (3.0 and 3.6 kcal/mol). In the first, the C_{re} = C_{si} Ph face is interacting with the enolate moiety, and in the second the

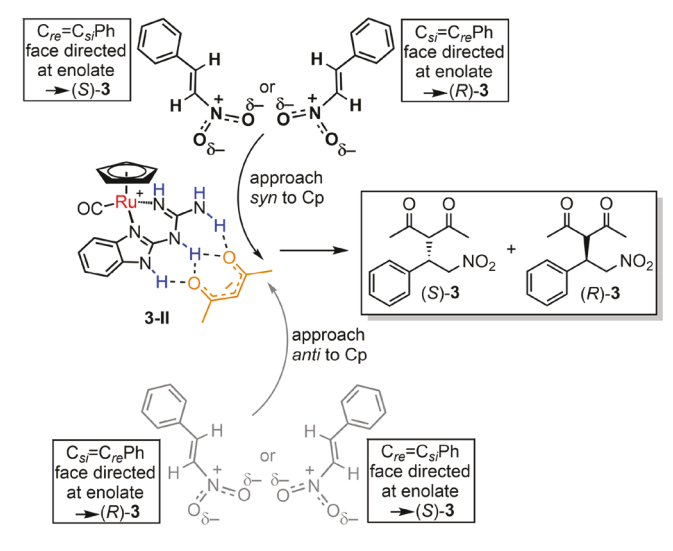


Figure 4. Limiting approaches of $trans-\beta$ -nitrostyrene to the deprotonated adduct of (S_{Ru}) -1⁺ and 2,4-pentanedione.

 C_{si} = C_{re} Ph face is interacting. Accordingly, subsequent carbon—carbon bond formation leads to opposite configurations at the new nitroalkene-derived stereocenter. These steps are mediated by π/π interactions as opposed to hydrogen bonding.

In Figure 6, the *anti* approach of *trans-\beta*-nitrostyrene to 3-II is similarly examined. Two lower lying adducts, 6-I and 6-I' (1.3 and 3.2 kcal/mol), are again found. In the first, the C_{si} = C_{re} Ph face is interacting with the enolate moiety, and in the second the C_{re} = C_{si} Ph face is interacting, leading to opposite product enantiomers.

Transition states could be located for each for the four initial adducts in Figures 5 and 6 and are designated TS_{CC}5, TS_{CC}5', TS_{CC}6', and TS_{CC}6'. These constitute the rate-determining steps on the carbon—carbon bond forming coordinate and afford the ylides 5-II, 5-II', 6-II, and 6-II'. The ylides feature

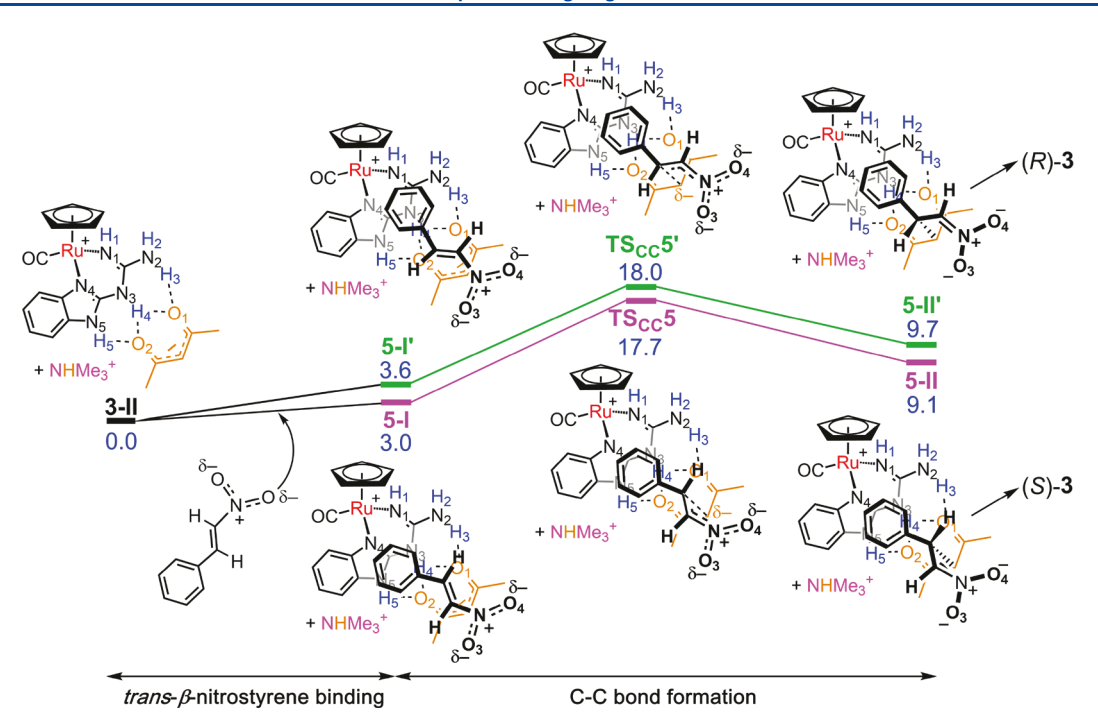


Figure 5. Relative free energy profiles ($\Delta G(CH_2Cl_2)$, kcal/mol) for species derived from (S_{Ru})-1⁺, 2,4-pentanedione, NMe₃, and trans-β-nitrostyrene, the last of which approaches syn to the cyclopentadienyl ligand. Selected distances (Å): 5-I, H₃-O₁ 1.73, H₄-O₁ 1.91, H₄-O₂ 2.19, H₅-O₂ 1.61; 5-I', H₃-O₁ 1.75, H₄-O₁ 1.86, H₄-O₂ 2.27, H₅-O₂ 1.59; TS_{CC}5, H₃-O₁ 1.81, H₄-O₁ 1.98, H₄-O₂ 2.20, H₅-O₂ 1.69; TS_{CC}5', H₃-O₁ 1.82, H₄-O₁ 1.92, H₄-O₂ 2.27, H₅-O₂ 1.70; 5-II, H₃-O₁ 1.87, H₄-O₁ 2.01, H₄-O₂ 2.25, H₅-O₂ 1.78; 5-II', H₃-O₁ 1.90, H₄-O₁ 1.90, H₄-O₂ 2.46, H₅-O₂ 1.78.

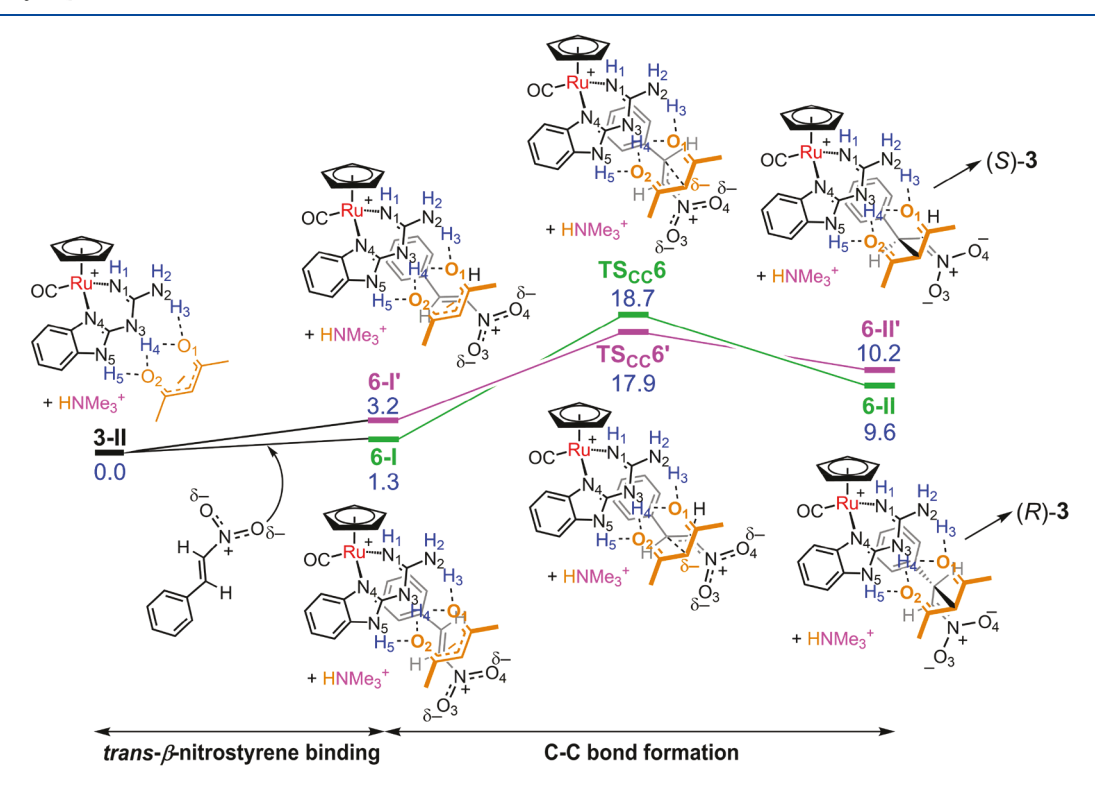


Figure 6. Relative free energy profiles (ΔG (CH₂Cl₂), kcal/mol) for species derived from (S_{Ru})-1⁺, 2,4-pentanedione, NMe₃, and trans-β-nitrostyrene the last of which approaches anti to the cyclopentadienyl ligand. Selected distances (Å): 6-I, H₃-O₁ 1.72, H₄-O₁ 1.88, H₄-O₂ 2.34, H₅-O₂ 1.59; 6-I', H₃-O₁ 1.73, H₄-O₁ 1.88, H₄-O₂ 2.37, H₅-O₂ 1.58; TS_{CC}6, H₃-O₁ 1.77, H₄-O₁ 1.93, H₄-O₂ 2.41, H₅-O₂ 1.67; TS_{CC}6', H₃-O₁ 1.76, H₄-O₁ 1.99, H₄-O₂ 2.28, H₅-O₂ 1.68; 6-II, H₃-O₁ 1.84, H₄-O₁ 1.97, H₄-O₂ 2.47, H₅-O₂ 1.75; 6-II', H₃-O₁ 1.84, H₄-O₁ 1.97, H₄-O₂ 2.46, H₅-O₂ 1.76.

negatively charged $C=N^+(-O^-)_2$ moieties and positively charged ruthenium fragments and are 9.1–10.2 kcal/mol less

stable than the educts. However, the energies plummet dramatically upon proton transfer from the protonated base

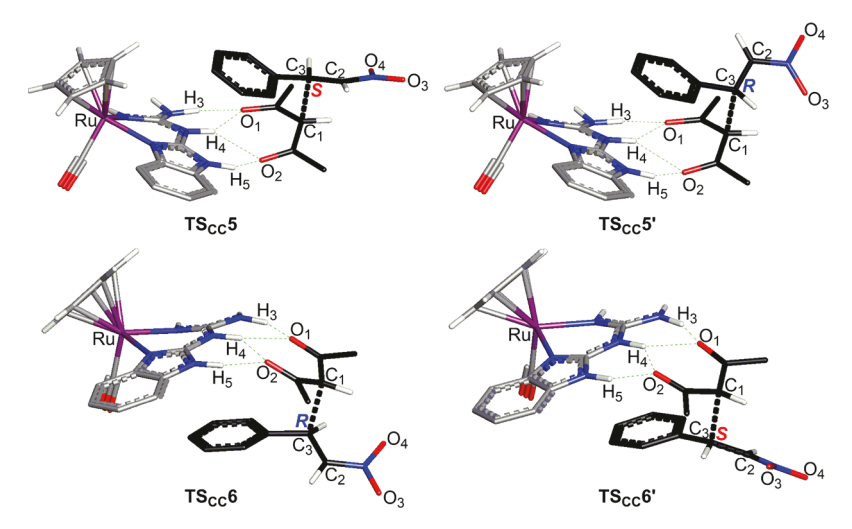


Figure 7. Alternative views of the transition states in Figures 5 and 6. Additional distances (Å): $5 \cdot I/TS_{CC}5/5 \cdot II$, $C_1 - C_3 \cdot 3.30/2.08/1.62$; $5 \cdot I'/TS_{CC}5'/5 \cdot II'$, $C_1 - C_3 \cdot 3.15/2.07/1.62$; $6 \cdot I/TS_{CC}6/6 \cdot II$, $C_1 - C_3 \cdot 3.38/2.07/1.62$.

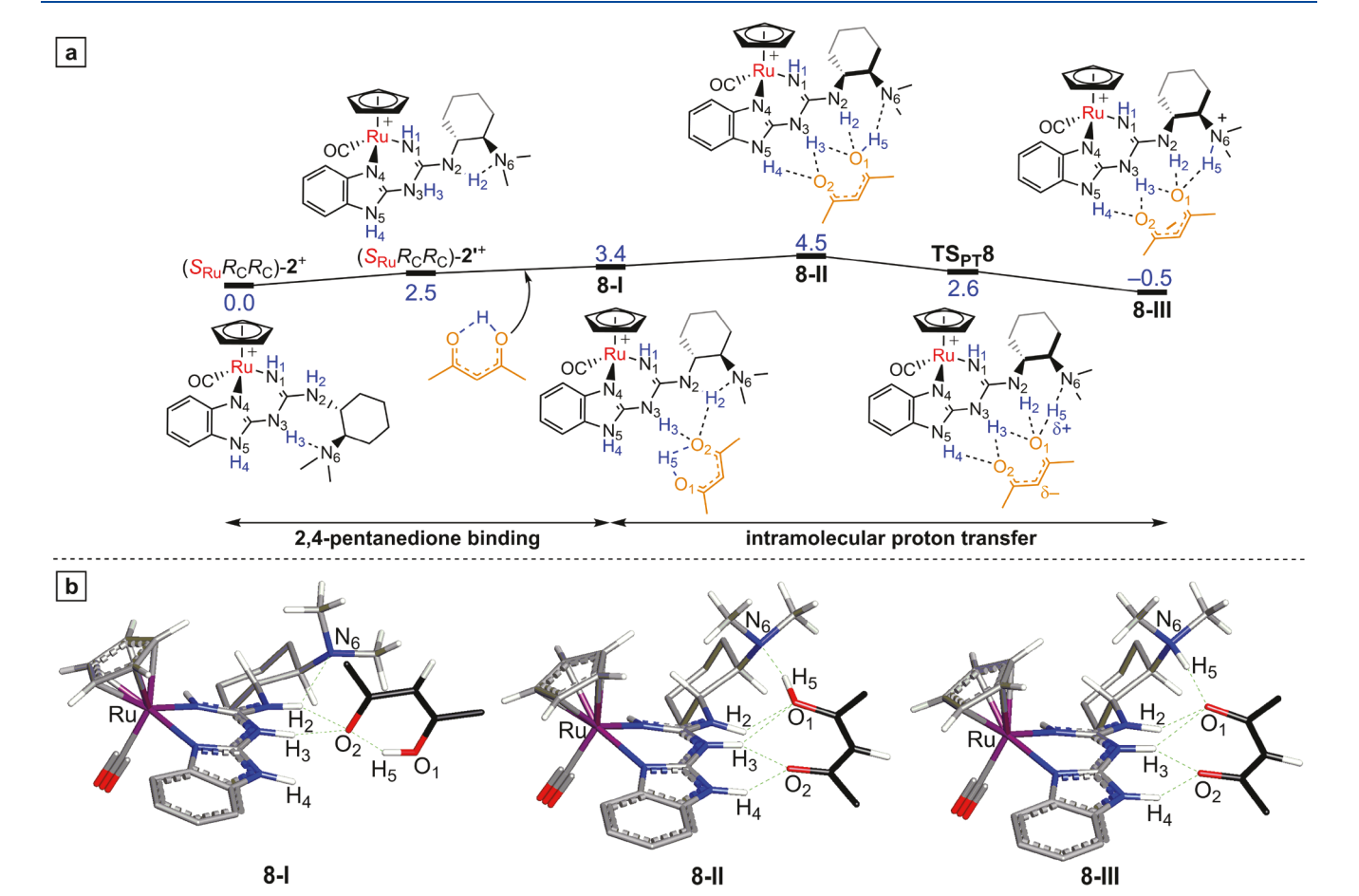


Figure 8. (a) Relative free energy profile ($\Delta G(CH_2Cl_2)$, kcal/mol) for binding of the enol of 2,4-pentanedione to ($S_{Ru}R_CR_C$)-2⁺ and subsequent intramolecular O/N proton transfer. (b) Optimized geometries of 8-I, 8-II, and 8-III. Selected distances (Å): ($S_{Ru}R_CR_C$)-2⁺, H₃-N₆ 1.58; ($S_{Ru}R_CR_C$)-2⁺, H₂-N₆ 2.12; 8-I, H₂-O₂ 2.18, H₂-N₆ 2.23, H₃-O₂ 1.78, H₅-O₁ 1.00, H₅-O₂ 1.61; 8-II, H₂-O₁ 2.06, H₃-O₁ 2.40, H₃-O₂ 1.85, H₄-O₂ 1.87, H₅-O₁ 1.04, H₅-N₆ 1.59; TS_{PT}8, H₂-O₁ 1.99, H₃-O₁ 2.45, H₃-O₂ 1.82, H₄-O₂ 1.86, H₅-O₁ 1.13, H₅-N₆ 1.40; 8-III, H₂-O₁ 1.82, H₃-O₁ 2.41, H₃-O₂ 1.81, H₄-O₂ 1.79, H₅-O₁ 1.63, H₅-N₆ 1.07.

HNMe₃⁺ to the C=N⁺($-O^-$)₂ moiety. Importantly, **5-II** and **6-II**' lead to (S)-**3**, whereas **5-II**' and **6-II** lead to (R)-**3** (all initially hydrogen bonded).

With reference to the lowest energy precursor 2-I (Figures 2 and 3), the energy barriers associated with TS_{CC}5, TS_{CC}5',

 $TS_{CC}6$, and $TS_{CC}6'$ are 18.0 (17.7 + 0.3), 18.3 (18.0 + 0.3), 19.0 (18.7 + 0.3), and 18.2 (17.9 + 0.3) kcal/mol, respectively. These values are quite close and are within commonly accepted "computational experimental error". In any case, those with activation energies of 18.0 and 18.2 kcal/mol lead

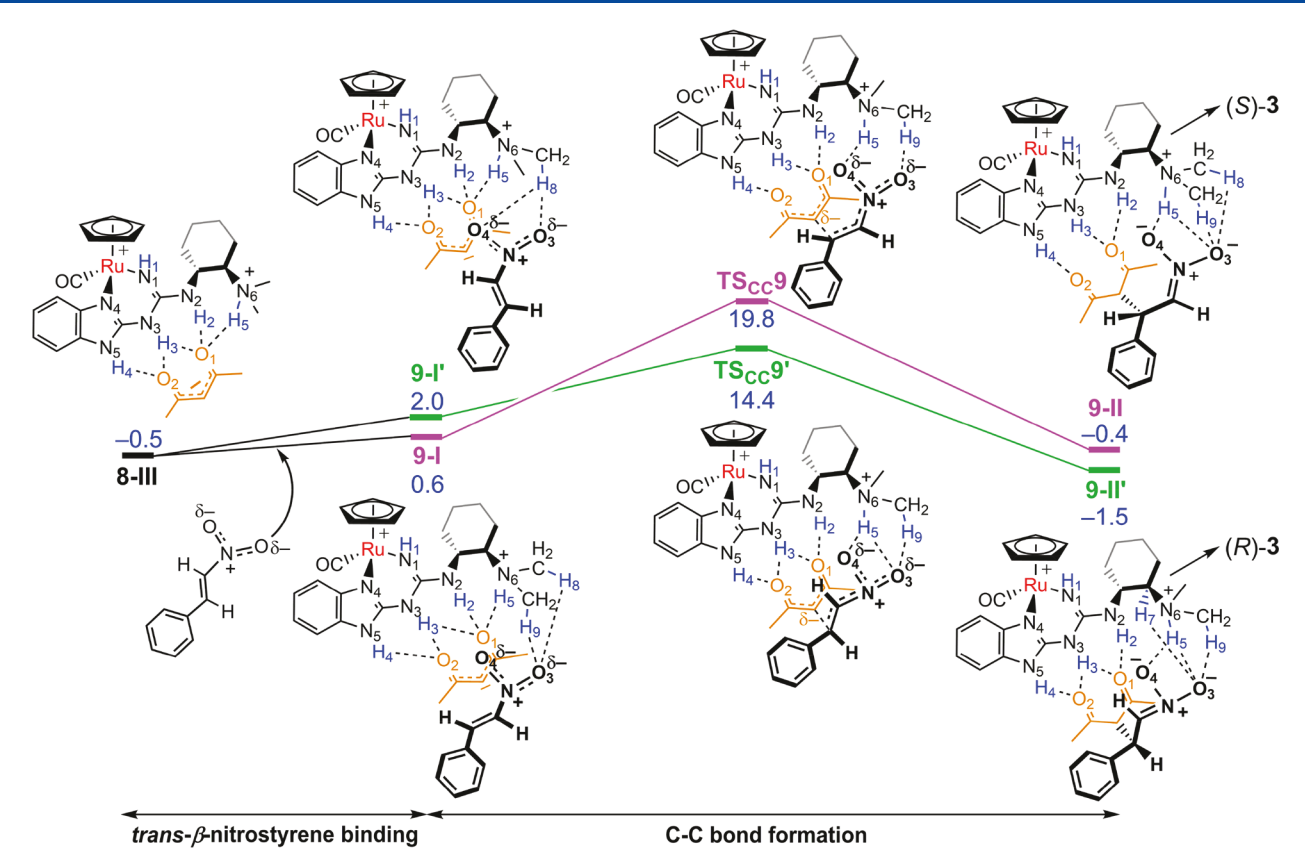


Figure 9. Relative free energy profiles ($\Delta G(\text{CH}_2\text{Cl}_2)$, kcal/mol) for species derived from ($S_{\text{Ru}}R_{\text{C}}R_{\text{C}}$)-2⁺, 2,4-pentanedione, and *trans-β*-nitrostyrene, the last of which approaches *syn* to the cyclopentadienyl ligand. Selected distances (Å): 9-I, H₂-O₁ 1.88, H₃-O₁ 2.26, H₃-O₂ 1.79, H₄-O₂ 1.80, H₅-O₁ 1.70, H₅-O₃ 2.85, H₅-O₄ 3.42, H₈-O₃ 2.43, H₉-O₃ 2.48; 9-I', H₂-O₁ 1.85, H₃-O₁ 2.31, H₃-O₂ 1.78, H₄-O₂ 1.79, H₅-O₁ 1.70, H₅-O₃ 2.92, H₅-O₄ 3.52, H₈-O₃ 2.57, H₈-O₄ 2.61; TS_{CC}9, H₂-O₁ 1.85, H₃-O₁ 1.77, H₄-O₂ 1.72, H₅-O₃ 2.79, H₅-O₄ 1.76, H₉-O₃ 2.33; TS_{CC}9', H₂-O₁ 1.71, H₃-O₁ 1.92, H₃-O₂ 2.34, H₄-O₂ 1.68, H₅-O₃ 2.39, H₅-O₄ 1.73, H₉-O₃ 2.63; 9-II, H₂-O₁ 2.07, H₃-O₁ 1.83, H₄-O₂ 1.85, H₅-O₃ 2.60, H₅-O₄ 1.59, H₈-O₃ 2.51, H₉-O₃ 2.28; 9-II', H₂-O₁ 1.82, H₃-O₁ 2.13, H₃-O₂ 2.25, H₄-O₂ 1.84, H₅-O₃ 2.33, H₅-O₄ 1.57, H₇-O₃ 2.56, H₉-O₃ 2.51.

to (S)-3 and those with activation energies of 18.3 and 19.0 kcal/mol to (R)-3. Hence, little or no enantioselectivity would be expected. A reviewer remarked that this outcome (in contrast to those for ($S_{Ru}R_CR_C$)- and ($R_{Ru}R_CR_C$)-2+PF₆-below) remains experimentally unverified due to the unavailability of enantiopure 1⁺. However, the pentaphenylcy-clopentadienyl analogue has, as described in the following paper, 5c been isolated in enantiopure form and catalyzes the addition of diethyl malonate to trans- β -nitrostyrene in a paltry 3% ee.

Alternative views of the transition states that focus on the syn/anti approaches of the nitroalkene to the GBI/enolate plane are provided in Figure 7. Some higher energy transition states in which $(S_{Ru})-1^+$ is hydrogen-bonded to both the enolate and $trans-\beta$ -nitrostyrene are depicted in Figures s2—s5 in the Supporting Information.

 $(S_{Ru}R_cR_c)$ -2+PF₆⁻: Binding of Educts. The additional GBI substituent and functionality in this complex and its diastereomer provide motifs similar to those in the widely employed bifunctional thiourea based hydrogen bond donor catalysts. In contrast to the results with 1+PF₆⁻ in the previous paper, 22 initial computations established that ion pairs in which the PF₆⁻ is solvent separated are comparable in energy to those where it hydrogen bonds to the cation (Figures s7–s10 in the Supporting Information). Nonetheless, the mechanism of Scheme 2 was probed with $(S_{Ru}R_cR_c)$ -2+, incorporating a hydrogen bond between the :NMe₂ lone pair

and the central NH of the triad that was observed crystallographically $(N_3H_3...N_6, 1.58 \text{ Å}; \text{ Figure 8a}).^{5b}$

In a step that ultimately aids substrate binding, the hydrogen bond in $(S_{Ru}R_CR_C)$ - 2^+ was replaced by one involving the proximal NH of the triad $(N_2H_2\cdots N_6,\ 2.12\ \text{Å})$, giving $(S_{Ru}R_CR_C)$ - $2'^+$ (Figure 8a). This rearrangement is 2.5 kcal/mol uphill, consistent with the presumably lower strength of the longer hydrogen bond. The new bond is in fact observed in crystal structures that contain the diastereomeric cation $(S_{Ru}R_CR_C)$ - 2^+ . The addition of both 2,4-pentanedione and trans- β -nitrostyrene to $(S_{Ru}R_CR_C)$ - $2'^+$ was then examined. In contrast to the sequence with monofunctional (S_{Ru}) - 1^+ , the :NMe₂ group of $(S_{Ru}R_CR_C)$ - 2^+ enables deprotonation of 2,4-pentanedione by the catalyst. This parallels results from a computational study involving the interaction of 2,4-pentanedione with a similarly functionalized thiourea.

Thus, a series of three energy minima, 8-I, 8-II, and 8-III, ensue as depicted in Figure 8a. The first features a cyclic enol ligand, in which the more weakly hydrogen bonded oxygen atom²⁴ interacts with two NH groups of the triad. In the second, the cyclic enol has isomerized to an acyclic enol, with the two oxygen atoms hydrogen bonding to all three NH groups of the triad; the OH group serves as a hydrogen bond donor to the :NMe₂ moiety. In the third, the hydrogen atom derived from the OH group covalently bonds to the :NMe₂ moiety while maintaining a hydrogen-bonding interaction with the oxygen atom. This species (8-III), the first with a

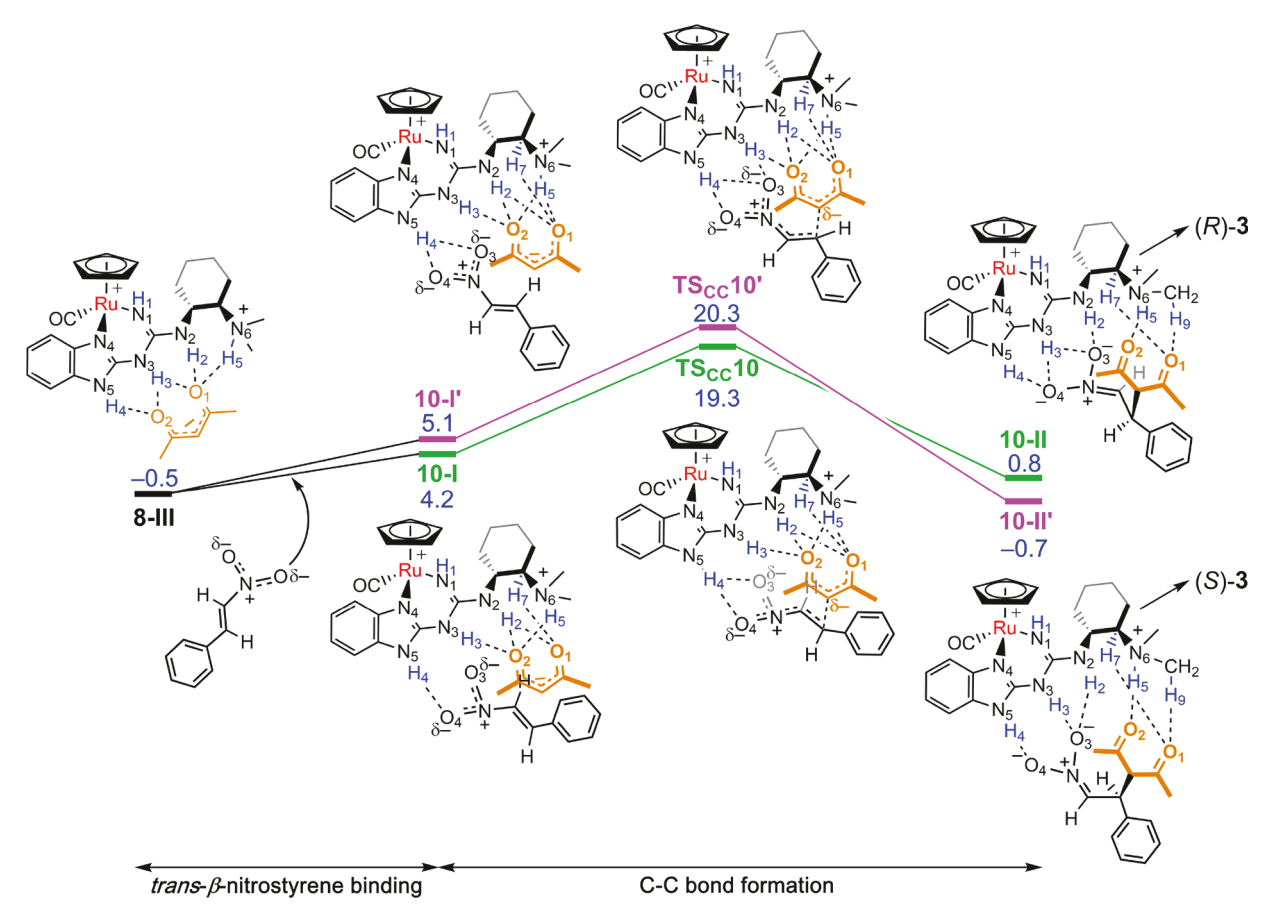


Figure 10. Relative free energy profiles ($\Delta G(\text{CH}_2\text{Cl}_2)$, kcal/mol) for species derived from ($S_{\text{Ru}}R_{\text{C}}R_{\text{C}}$)-2⁺, 2,4-pentanedione, and *trans-β*-nitrostyrene, the last of which approaches *anti* to the cyclopentadienyl ligand. Selected distances (Å): 10-I, H₂-O₁ 1.79, H₂-O₂ 2.44, H₃-O₂ 1.78, H₄-O₃ 2.65, H₄-O₄ 1.90, H₅-O₂ 1.69, H₇-O₁ 2.27; 10-I′, H₂-O₁ 1.81, H₂-O₂ 2.51, H₃-O₂ 1.72, H₄-O₃ 2.57, H₄-O₄ 1.92, H₅-O₁ 2.50, H₅-O₂ 1.70, H₇-O₁ 2.27; TS_{CC}10, H₂-O₁ 2.04, H₂-O₂ 2.41, H₃-O₂ 1.84, H₄-O₃ 2.49, H₄-O₄ 1.78, H₅-O₁ 2.49, H₅-O₂ 1.82, H₇-O₁ 2.21; TS_{CC}10′, H₂-O₁ 2.00, H₂-O₂ 2.59, H₃-O₃ 1.82, H₄-O₃ 2.41, H₄-O₄ 1.79, H₅-O₁ 2.49, H₅-O₂ 1.72, H₇-O₁ 2.19; 10-II, H₂-O₃ 1.74, H₃-O₃ 2.44, H₃-O₄ 1.58, H₄-O₄ 2.61, H₅-O₂ 1.80, H₇-O₁ 2.52, H₉-O₁ 2.33; 10-II′, H₂-O₃ 2.09, H₃-O₃ 1.56, H₄-O₄ 1.74, H₅-O₂ 1.76, H₇-O₁ 2.39, H₉-O₁ 2.34.

deprotonated dione ligand, is downhill from the educts by -0.5 kcal/mol. Hence, 0.5 kcal/mol must be added to the $\Delta G(\mathrm{CH_2Cl_2})$ value of any subsequently derived transition state to obtain a free energy of activation (such intermediates were not encountered with the diastereomeric catalyst; see below).

Alternative representations of 8-I, 8-II, and 8-III are provided in Figure 8b. These emphasize the increasing elevation of the :NMe₂ group above the GBI plane, achieved by simply rotating about the cyclohexyl—NH($C_{\rm sp2}$) bond. They also illustrate the deviation of the plane of the enol or enolate from the GBI plane. Some higher energy structures in which the :NMe₂ group is rotated below the plane are shown in Figure s11 in the Supporting Information.

The rate-determining step in Figure 8 is the conversion of 8-II to 8-III. The structure of the transition state, which involves O···H···N proton transfer, is shown as $TS_{PT}8$. The overall energy barrier is only 2.6 kcal/mol. Although the free energy of $TS_{PT}8$ is lower than that of 8-II, the electronic energy of $TS_{PT}8$ is slightly higher (-15.3 vs -15.6 kcal/mol; Table s16 in the Supporting Information), a trend that has ample precedent. In any case, the energy barrier is much less than that for (S_{Ru}) -1⁺ and the external base NMe₃ in Figure 3.

Some readers may have noted the use of 2,4-pentanedione in Figures 2 and 3 but the cyclic enol tautomer in Figure 8a. As shown in Figure s12 in the Supporting Information, replacing

the enol ligand by the dione in Figure 8a affords significantly higher energy adducts. The binding of $trans-\beta$ -nitrostyrene to $(S_{\rm Ru}R_{\rm C}R_{\rm C})$ -2' was also examined (Figures s13–s15 in the Supporting Information). However, the most stable adducts were 4.7–5.0 kcal/mol uphill, in comparison to a maximum of 4.5 kcal/mol for all of the species on the reaction coordinate in Figure 8, including transition states.

($S_{Ru}R_cR_c$)-2*: Carbon–Carbon Bond Formation. Interactions of 8-III and *trans-β*-nitrostyrene were probed computationally as for 3-II above. As in Figure 5, those involving approaches *syn* to the cyclopentadienyl ligand were considered first. As shown by 9-I and 9-I' in Figure 9, the most favorable initial adducts exhibited 2-fold hydrogen bonding between one or both oxygen atoms of the nitro group, and NCH₂-H linkages from one or both *N*-methyl groups. The NCH₂H···O distances (2.43–2.61 Å) were considerably longer than most of the NH···O hydrogen bonds noted above. In 9-I, the C_{re} = C_{si} Ph face is interacting with the enolate moiety, and in 9-I' the C_{si} = C_{re} Ph face is interacting. Hence, opposite enantiomers of 3 should result.

Quite different structures were computed when $trans-\beta$ -nitrostyrene was restricted to approaching anti to the cyclopentadienyl ligand. As shown by **10-I** and **10-I**′ in Figure 10, the nitro groups now interact with the opposite terminus of the substituted GBI ligand, hydrogen bonding to the NH

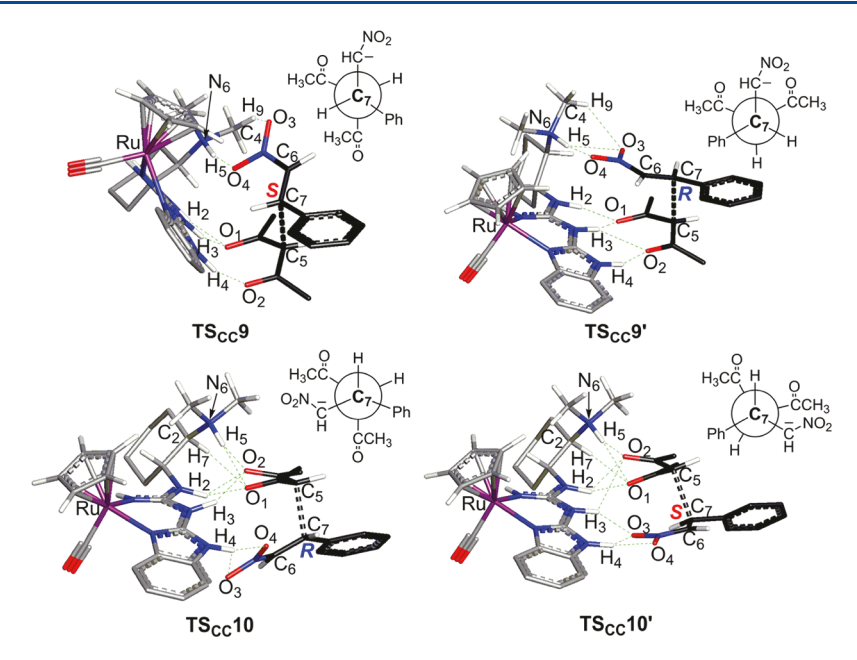


Figure 11. Alternative views of the transition states in Figures 9 and 10. Additional distances (Å): 9-I/TS_{CC}9/9-II, C_5 - C_7 3.79/2.27/1.57; 9-I'/TS_{CC}9'/9-II', C_5 - C_7 3.34/2.25/1.59; 10-I/TS_{CC}10/10-II, C_5 - C_7 3.21/2.14/1.58; 10-I'/TS_{CC}10'/10-II', C_5 - C_7 3.90/2.24/1.57. H- C_5 - C_7 -H torsion angle (deg): TS_{CC}9, 176.9; TS_{CC}9', 55.4; TS_{CC}10, 63.5; TS_{CC}10', 143.2.

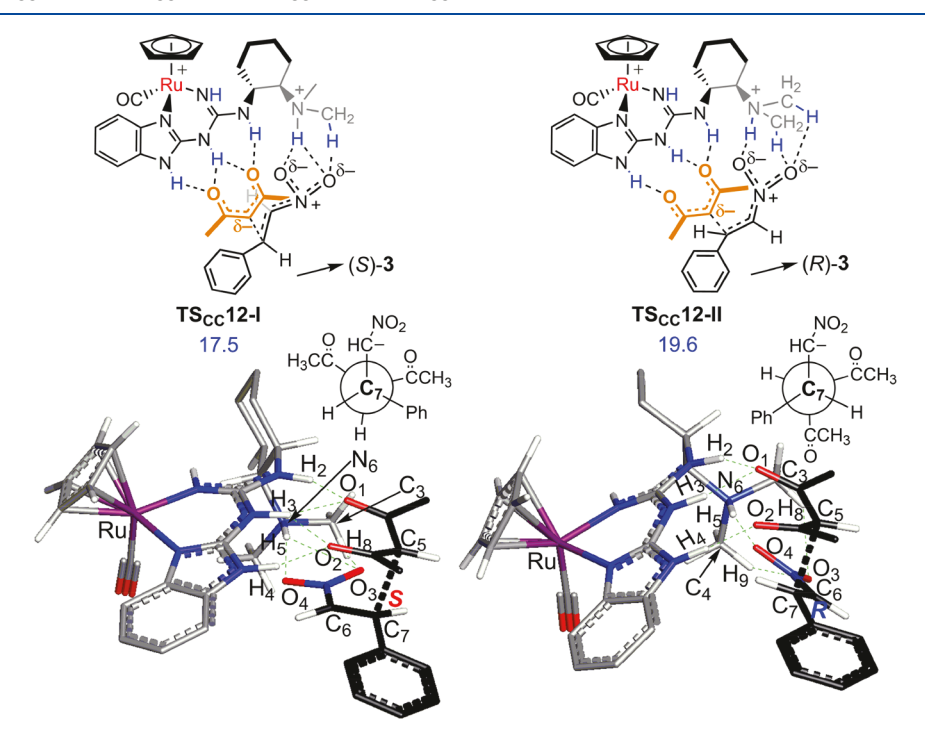


Figure 12. Additional transition states and $\Delta G(CH_2Cl_2)$ values (kcal/mol) calculated from the starting materials for Figures 9 and 10. Selected distances (Å): TS_{CC}12-I, H₂-O₁ 1.78, H₃-O₁ 1.79, H₃-O₂ 2.59, H₄-O₂ 1.69, H₅-O₃ 2.57, H₅-O₄ 1.77, H₈-O₃ 2.50, C₅-C₇ 2.23; TS_{CC}12-II, H₂-O₁ 1.87, H₃-O₁ 1.71, H₄-O₂ 1.67, H₅-O₃ 2.80, H₅-O₄ 1.79, H₈-O₃ 2.34, H₉-O₃ 2.38, C₅-C₇ 2.24. H-C₅-C₇-H torsion angle (deg): TS_{CC}12-I, 47.4; TS_{CC}12-II, 175.6.

group of the N_s-H_4 linkage. The enolate ligands maintain one hydrogen bond with the central N_3-H_3 linkage but otherwise slither over, generating multiple hydrogen bonds with the 1,2-diaminocyclohexane ring. In 10-I, the $C_{si}=C_{re}$ Ph face is interacting with the enolate moiety, and in 10-I' the $C_{re}=C_{si}$ Ph face is interacting.

Transition states could be located for each for the four initial adducts in Figures 9 and 10 and are designated $TS_{CC}9$, $TS_{CC}9'$, $TS_{CC}10$, and $TS_{CC}10'$. Alternative views are presented

in Figure 11, together with Newman projections down the newly forming carbon—carbon bonds (C_7-C_5) or $O_2NCH-(Ph)HC-CH(COCH_3)_2$. These constitute the rate-determining steps and afford 9-II, 9-II', 10-II, and 10-II', which are hydrogen-bonded adducts of the product 3. To obtain activation energies, 0.5 kcal/mol must be added to the $\Delta G(CH_2Cl_2)$ values in Figures 9 and 10, reflecting the energy of the global minimum 8-III (-0.5 kcal/mol). This gives 20.3 $(TS_{CC}9; 19.8 + 0.5), 14.9 (TS_{CC}9'; 14.4 + 0.5), 19.8 (TS_{CC}10;$

19.3 + 0.5), and 20.8 ($TS_{CC}10'$; 20.3 + 0.5) kcal/mol. Given the considerably lower activation energy for $TS_{CC}9'$, it should be the dominant reaction channel and indeed leads to (R)-3 in agreement with experiment.

Additional comparisons are provided by the Newman projections in Figure 11. For example, the C_7 – C_5 substituents in the highest energy species $\mathbf{TS_{CC}10'}$ are nearly eclipsed (X– C_7 – C_5 –Y torsion angles for synperiplanar X/Y: 27, 26, 15°), whereas those in the other transition states are staggered. In terms of factors favoring $\mathbf{TS_{CC}9'}$ over $\mathbf{TS_{CC}9}$, both the enolate and NO₂ oxygen atoms are more extensively hydrogen bonded in the former. Although comparisons of $\mathbf{TS_{CC}9'}$ with $\mathbf{TS_{CC}10}$ and $\mathbf{TS_{CC}10'}$ are more challenging due to the lower structural homology, transition states in which the NO₂ oxygen atoms no longer bind to the HNMe₂⁺ moiety always exhibit higher activation energies.

Eight additional transition states derived from $(S_{Ru}R_CR_C)$ -2⁺ could be located, as depicted in Figures s16, s17, s19, and s20 in the Supporting Information. For the two shown in Figure 12, TS_{CC} 12-I and TS_{CC} 12-II, the $\Delta G(CH_2Cl_2)$ values (17.5 and 19.6 kcal/mol) also represent activation energies, as there are no intermediates like 8-III with energies lower than those of the educts. These constitute the only other transition states with activation energies lower than the highest energy in Figures 9–11 (TS_{CC} 10', 20.3 + 0.5 kcal/mol). The second, TS_{CC} 12-II, leads to (R)-3 and shares several features with TS_{CC} 9 but involves the opposite C_{si} = C_{re} Ph enantioface of trans-β-nitrostyrene and addition anti to the cyclopentadienyl ligand. Since it has a much higher activation energy in comparison to TS_{CC} 9' (14.4 + 0.5 kcal/mol), the dominant channel to (R)-3, it is not further analyzed.

The activation energy for $TS_{CC}12$ -I (17.5 kcal/mol) renders it the most favorable channel to (S)-3. Here, the $C_{re}=C_{si}Ph$ face of trans- β -nitrostyrene adds from a direction anti to the cyclopentadienyl ligand, as opposed to the $C_{si}=C_{re}Ph$ face adding syn as in $TS_{CC}9'$. The lower activation energy for $TS_{CC}9'$ versus $TS_{CC}12$ -I appears to be due to a number of factors. The hydrogen-bonding motifs are similar, but the distances involving the NO_2 oxygen atoms and $HNMe_2^+$ moiety in $TS_{CC}9'$ are generally shorter (1.73 vs 1.77 Å; 2.39 vs 2.57 Å; 2.63 vs 2.50 Å). The shortest $O\cdots HNMe_2$ linkage in $TS_{CC}9'$ exhibits a higher degree of linearity (164.9° vs 156.4°). Also, the $H-C_7-C_5-H$ torsion angle of $TS_{CC}9'$ indicates a more staggered arrangement of substituents (55.4° vs 47.4°).

Furthermore, the 1,2-diaminocyclohexane rings adopt much different conformations in $TS_{CC}9'$ and $TS_{CC}12$ -I. To help gauge this effect, the substrates and the metal fragment were removed to give the free substituted GBI ligands and their :NMe₂-protonated forms. As illustrated in Figure 13, the conformations differ by a ca. 180° rotation about the cyclohexyl-NH(C_{sp}^2) bond. That in $TS_{CC}12$ -I (B) is 1.2–1.6 kcal/mol less stable than that in $TS_{CC}9'$ (A). This can be ascribed to interactions involving two axial C-H groups of the cyclohexane ring and the C=NH substituent of the NH group. The stability difference increases to 2.1 kcal/mol when the substrates are added.²⁹

In any case, from a computational standpoint, the high enantioselectivities for the additions of 1,3-dicarbonyl compounds to trans- β -nitrostyrene catalyzed by $(S_{Ru}R_CR_C)$ - $2^+PF_6^-$ in Schemes 1 and 2 largely derive from two competing transition states with a 2.6 kcal/mol difference in free energies. This agrees well with the >99:<1 to 92:8 product enantiomer ratios.

Figure 13. Differences in electronic energies for GBI ligands excised from the transition states $TS_{CC}9'$ and $TS_{CC}12$ -I.

 $(R_{\rm Ru}R_{\rm c}R_{\rm c})$ -2*: Carbon–Carbon Bond Formation. Given the comparable enantioselectivities and identical product configurations obtained with the diastereomeric catalysts $(S_{\rm Ru}R_{\rm c}R_{\rm c})$ - and $(R_{\rm Ru}R_{\rm c}R_{\rm c})$ -2*PF $_6$ ⁻ (Schemes 1 and 2), it would not be surprising to compute similar sets of transition states. The former complex can be converted to the latter by simply exchanging the positions of the cyclopentadienyl and carbonyl ligands. Both ligands are remote from the sites where the catalyst and educts interact, as well as the 1,2-diaminocyclohexane moiety. There are no van der Waals contacts in any of the structures computed above or in the crystal structures. ^{5b}

Accordingly, through similar procedures, the transition states and $\Delta G(\mathrm{CH_2Cl_2})$ values depicted in Figure 14 were computed. In this series, the latter are equivalent to the free energies of activation. There are four transition states, $TS_{CC}13\text{-I}$ through $TS_{CC}13\text{-IV}$, corresponding to those in Figures 8–10, and two more, $TS_{CC}13\text{-V}$ and $TS_{CC}13\text{-VI}$, corresponding to those in Figure 12. The complete reaction coordinates are illustrated in Figures s22–s30 in the Supporting Information. Now the HNMe₂⁺ units of the 1,2-diaminocyclohexane moieties are anti as opposed to syn to the cyclopentadienyl ligands for $TS_{CC}13\text{-IV}$ through $TS_{CC}13\text{-IV}$, and syn as opposed to anti for $TS_{CC}13\text{-VI}$ and $TS_{CC}13\text{-VI}$. This is a logical consequence of the "cyclopentadienyl/carbonyl flip" noted in the preceding paragraph.

Here, the lowest energy transition state, TS_{CC}13-II, leads to the major product enantiomer, (R)-3 (addition of the C_{si} C_{re} Ph face anti to the cyclopentadienyl ligand). It features exactly the same grouping of hydrogen bonds as was found for the lowest energy transition state derived from the diastereomer $(S_{Ru}R_CR_C)$ -2⁺ in Figures 8–10 $(TS_{CC}9')$. Their relative energies (15.1 vs 14.9 kcal/mol) represent the cost of the "cyclopentadienyl/carbonyl flip". The two lowest energy transition states that lead to the minor product enantiomer, (S)-3, are analogous to those in Figures 8–10 (TS_{CC}13-V, comparable to TS_{CC}12-I (17.2 vs 17.5 kcal/mol) and involving addition of the C_{re} = C_{si} Ph face syn to the cyclopentadienyl ligand; TS_{CC}13-I, comparable to TS_{CC}9 (18.4 vs 20.3 kcal/ mol) and involving addition of the $C_{re} = C_{si}Ph$ face anti to the cyclopentadienyl ligand). In any case, the high enantioselectivities obtained with $(R_{Ru}R_CR_C)-2^+PF_6^-$ in Schemes 1 and 2 largely derive from two competing transition states with a computed 2.1 kcal/mol difference in activation energies ($TS_{CC}13$ -II and $TS_{CC}13$ -V).

DISCUSSION

The data in Figures 5 and 6 show that enantiopure 1⁺PF₆⁻ would be expected to catalyze additions of 1,3-dicarbonyl

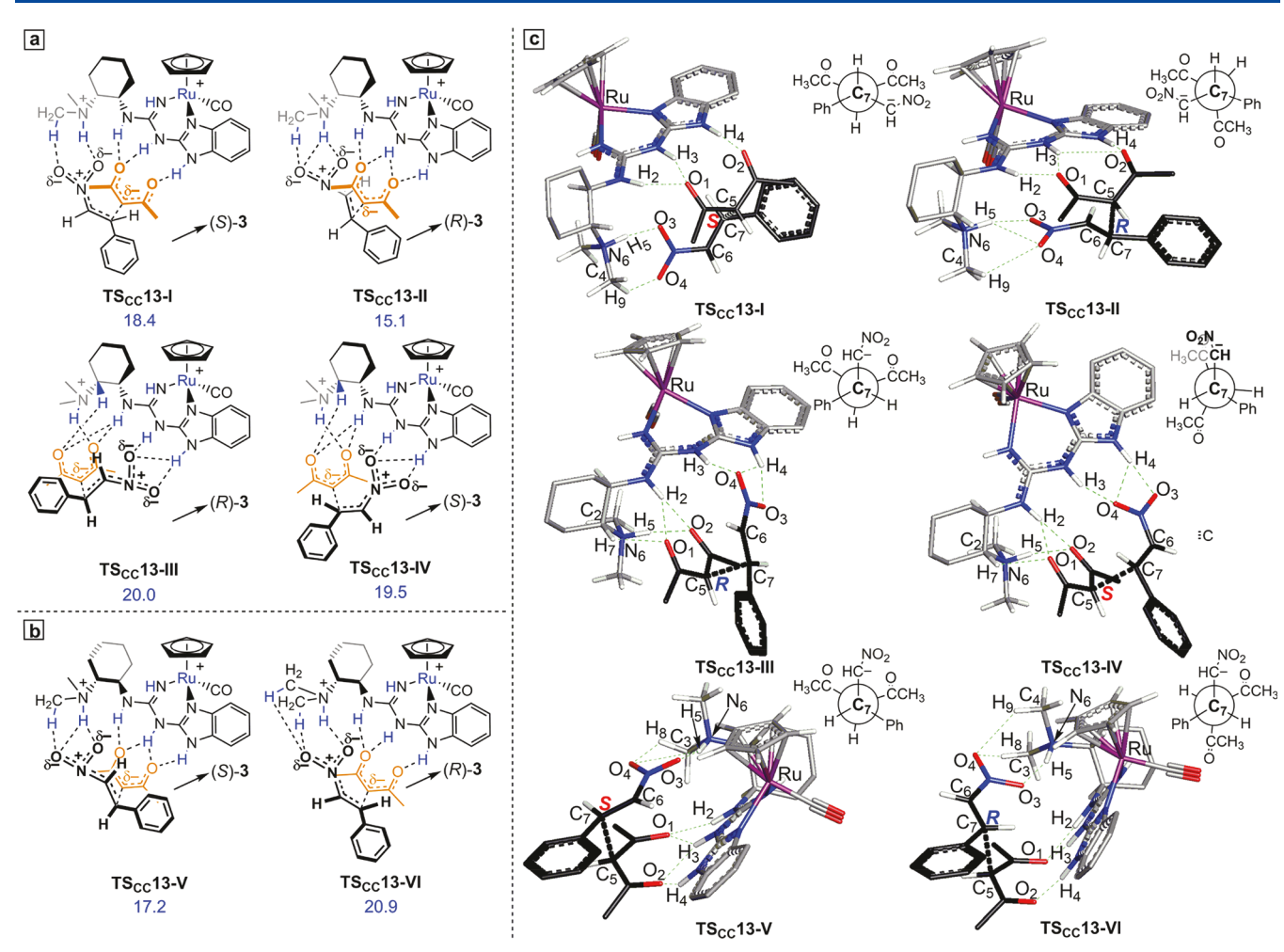


Figure 14. Relative free energies ($\Delta G(CH_2Cl_2)$, kcal/mol) of additional transition states for species derived from ($R_{Ru}R_CR_C$)-2+, 2,4-pentanedione, and trans-β-nitrostyrene with the HNMe₂+ moiety (a) anti or (b) syn to the cyclopentadienyl ligand. (c) Optimized geometries of the transition states. Selected distances (Å): TS_{CC}13-I, H₂-O₁ 1.87, H₃-O₁ 1.73, H₄-O₂ 1.68, H₅-O₃ 1.76, H₉-O₄ 2.27, C₅-C₇ 2.24; TS_{CC}13-II, H₂-O₁ 1.78, H₃-O₁ 1.79, H₃-O₂ 2.61, H₄-O₂ 1.68, H₅-O₃ 1.75, H₅-O₄ 2.50, H₉-O₄ 2.49, C₅-C₇ 2.24; TS_{CC}13-III, H₂-O₁ 1.96, H₂-O₂ 2.53, H₃-O₄ 1.79, H₄-O₃ 1.83, H₄-O₄ 2.53, H₅-O₂ 1.70, H₇-O₁ 2.22, C₅-C₇ 2.24; TS_{CC}13-IV, H₂-O₁ 1.89, H₂-O₂ 2.52, H₃-O₄ 1.77, H₄-O₃ 1.74, H₄-O₄ 2.50, H₅-O₂ 1.72, H₇-O₁ 2.23, C₅-C₇ 2.22; TS_{CC}13-V, H₂-O₁ 1.78, H₃-O₁ 2.26, H₃-O₂ 1.97, H₄-O₂ 1.75, H₅-O₃ 1.72, H₅-O₄ 2.57, H₈-O₄ 2.50, C₅-C₇ 2.25; TS_{CC}13-VI, H₂-O₁ 1.86, H₃-O₁ 1.73, H₄-O₂ 1.68, H₅-O₃ 1.78, H₈-O₄ 2.42, H₉-O₄ 2.37, C₅-C₇ 2.25. H-C₅-C₇-H torsion angle (deg): TS_{CC}13-I, 174.5; TS_{CC}13-II, 48.1; TS_{CC}13-III, 71.1; TS_{CC}13-IV, 134.4; TS_{CC}13-V, 49.7; TS_{CC}13-VI, 175.3.

compounds to $trans-\beta$ -nitrostyrene or related nitroalkenes with little or no enantioselectivity. It was not possible to test this experimentally, due to our inability to resolve racemic $\mathbf{1}^+\mathrm{PF}_6^-$. However, the conclusion makes intuitive sense, given the appreciable distance between the ruthenium stereocenter and the locus of reaction on the remote side of the GBI ligand and is buttressed by data for the enantiopure pentaphenylcyclopentadienyl analogue in the following paper. Sc Accordingly, the carbon stereocenters and added functionality in $(S_{\mathrm{Ru}}R_{\mathrm{C}}R_{\mathrm{C}})$ -and $(R_{\mathrm{Ru}}R_{\mathrm{C}}R_{\mathrm{C}})$ - $\mathbf{2}^+\mathrm{PF}_6^-$ play critical roles in achieving highly enantioselective catalysis.

What are these critical roles? Given the close relationships of the transition states for the diastereomeric catalysts (*vide supra*), only ($S_{Ru}R_{C}R_{C}$)-2⁺PF₆⁻ is treated here. For some stereoselective processes, one can point to a dominant interaction or causative feature, whereas in other cases a number of smaller factors come into play. The activation energies for the most favorable transition states leading to the addition product (R)-3 (major enantiomer) and (S)-3, $TS_{CC}9'$, and $TS_{CC}12$ -I (Figures 9, 10, and 12) differ by 2.6 kcal/mol (14.4 + 0.5 vs 17.5 kcal/mol). As framed in the

Results, the energy difference appears to derive from a combination of factors.

In both cases, a Brønsted acidic $HNMe_2^+$ moiety (attached to one of the carbon stereocenters) is generated by deprotonation of the 1,3-dicarbonyl compound. This in turn mediates the introduction of the nitrostyrene via hydrogen bonding. In $TS_{CC}9'$, the conformation of the cyclohexane ring places the $HNMe_2^+$ moiety above the plane of the GBI ligand, whereas in $TS_{CC}12$ -I it is below. In the first case, the C_{si} = C_{re} Ph nitrostyrene face is attacked from a direction syn to the cyclopentadienyl ligand (Figures 9 and 11), and in the second the C_{re} = C_{si} Ph face is attacked from a direction anti to the cyclopentadienyl ligand (Figure 12).

Factors noted above include the shorter lengths and more linear angles associated with key hydrogen bonds in $TS_{CC}9'$ and more staggered torsion angles. However, roughly half of the difference in activation energies appears to derive from unfavorable steric interactions involving two axial C–H groups of the 1,2-diaminocyclohexane moiety of $TS_{CC}12$ -I (Figure 13). One can then propose that, in order for $TS_{CC}12$ -I to generate the hydrogen-bonding interactions necessary to

activate the substrates and effect catalysis, it is necessary to introduce some destabilizing strain involving one of the cyclohexane ring substituents, raising the energy relative to $TS_{CC}9'$.

Since the ruthenium configuration has virtually no influence upon the product configurations and ee values, one can question whether the metal stereocenter is needed at all. In this context, parallel reactions have been conducted with the free ligand (R_CR_C) -GBI-CH $(CH_2)_4$ CHNMe₂, which corresponds to **A-b** in Figure 13. These give much lower rates and enantioselectivities, with an average ee value of 34% for the substrates in Scheme 1. We have speculated that the ability of ruthenium to "preorganize" GBI ligands via chelation into geometrically well defined NH triads is a critical aspect of this difference.

Some other chiral catalysts for additions of 1,3-dicarbonyl compounds to nitroalkenes merit note. For example, Takemoto developed the bifunctional thiourea based species 14 shown in Figure 15. 8b,26 This bears an obvious relationship to

Figure 15. Other relevant bifunctional hydrogen bond donor catalysts and transition state assemblies.

 $(S_{\rm Ru}R_{\rm C}R_{\rm C})$ - and $(R_{\rm Ru}R_{\rm C}R_{\rm C})$ -2+PF₆⁻, and he has proposed the transition state assembly shown in TS_{CC}15, which has garnered support in some computational studies.³⁰ Many groups have subsequently developed related bifunctional catalysts,^{2d} and we single one out by Soós $(16)^{31}$ as he later collaborated with Pápai in computational papers.²⁷ Their DFT calculations implicated the assembly TS_{CC}15' for the Takemoto system. This bears a marked conceptual relationship to our transition states TS_{CC}9' (Figure 9) and TS_{CC}13-II (Figure 14). The Pápai model has received strong support from additional studies,³² and related transition states have been calculated for other types of addition reactions.³³

In conclusion, the chiral cation 1^+ and 2,4-pentanedione readily associate via NH···O hydrogen bonds, but an external base NR₃ is required to generate an enolate. The *trans-\beta*-nitrostyrene then associates with the enolate in a π/π motif, but there is little selectivity with respect to the C=CPh or enolate π face, leading to racemic addition products. In

contrast, following the initial bonding of the dione to the diastereomeric cations $(S_{Ru}R_{C}R_{C})-2^{+}$ and $(R_{Ru}R_{C}R_{C})-2^{+}$, a proton is rapidly transferred to the internal :NMe₂ moiety, giving an enolate and a Brønsted acidic HNMe₂⁺ moiety. The latter, which is attached to a carbon stereocenter, mediates the introduction of the nitrostyrene such that in the rate-determining carbon—carbon bond forming step, the proximal π face of the enolate attacks the C_{si} — C_{re} Ph face. This leads to an addition product with an R configuration. Thus, the carbon stereocenters in the catalyst control the product configuration, in agreement with Schemes 1 and 2. These findings suggest a number of strategies for further optimizing the rates and enantioselectivities associated with this catalyst family. These are offered as speculations in the following paper, which details an alternative empirical experimental approach. Sc

ASSOCIATED CONTENT

Supporting Information

The Supporting Information is available free of charge at https://pubs.acs.org/doi/10.1021/acs.organomet.0c00072.

Free energy profiles, optimization geometries, computational details, verification of the gas- and solution-phase optimization, and tables of energies (PDF)

Optimized structure files (XYZ)

AUTHOR INFORMATION

Corresponding Authors

Michael B. Hall — Department of Chemistry, Texas A&M University, College Station, Texas 77843-3012, United States; orcid.org/0000-0003-3263-3219; Email: mbhall@tamu.edu

John A. Gladysz — Department of Chemistry, Texas A&M University, College Station, Texas 77843-3012, United States; orcid.org/0000-0002-7012-4872; Email: gladysz@ mail.chem.tamu.edu

Authors

Taveechai Wititsuwannakul — Department of Chemistry, Texas A&M University, College Station, Texas 77843-3012, United States

Tathagata Mukherjee — Department of Chemistry, Texas A&M University, College Station, Texas 77843-3012, United States; orcid.org/0000-0002-6369-8923

Complete contact information is available at: https://pubs.acs.org/10.1021/acs.organomet.0c00072

Notes

The authors declare no competing financial interest.

ACKNOWLEDGMENTS

The authors thank the Welch Foundation (Grants A-1656 (J.A.G.) and A-0648 (M.B.H.)) and the U.S. National Science Foundation (CHE-1664866 (M.B.H.)) for support, the Laboratory for Molecular Simulation and Texas A&M High Performance Research Computing Facility for computational resources, and Dr. Lisa M. Pérez for helpful discussions.

REFERENCES

(1) (a) Dalko, P. I.; Moisan, L. In the Golden Age of Organocatalysis. *Angew. Chem., Int. Ed.* **2004**, 43, 5138–5175. Im Goldenen Zeitalter der Organokatalyse *Angew. Chem.* **2004**, 116, 5248–5286. (b) Volla, C. M. R.; Atodiresei, I.; Rueping, M. Catalytic

- C-C Bond-Forming Multi-Component Cascade or Domino Reactions: Pushing the Boundaries of Complexity in Asymmetric Organocatalysis. *Chem. Rev.* **2014**, *114*, 2390–2431. (c) Berkessel, A.; Gröger, H. *Asymmetric Organocatalysis: From Biomimetic Concepts to Applications in Asymmetric Synthesis*; Wiley-VCH: Weinheim, 2005. (d) Scheffler, U.; Mahrwald, R. Recent Advances in Organocatalytic Methods for Asymmetric C-C Bond Formation. *Chem. Eur. J.* **2013**, *19*, 14346–14396.
- (2) (a) Taylor, M. S.; Jacobsen, E. N. Asymmetric Catalysis by Chiral Hydrogen-Bond Donors. *Angew. Chem., Int. Ed.* **2006**, *45*, 1520–1543. Asymmetrische Katalyse durch chirale Wasserstoffbrückendonoren. *Angew. Chem.* **2006**, *118*, 1550–1573. (b) Doyle, A. G.; Jacobsen, E. N. Small-Molecule H-Bond Donors in Asymmetric Catalysis. *Chem. Rev.* **2007**, *107*, 5713–5743. (c) Yu, X.; Wang, W. Hydrogen-Bond-Mediated Asymmetric Catalysis. *Chem. Asian J.* **2008**, *3*, 516–532. (d) Held, F. E.; Tsogoeva, S. B. Asymmetric cycloaddition reactions catalyzed by bifunctional thiourea and squaramide organocatalysts: recent advances. *Catal. Sci. Technol.* **2016**, *6*, 645–667.
- (3) (a) Ghosh, S. K.; Lewis, K. G.; Kumar, A.; Gladysz, J. A. Syntheses of Families of Enantiopure and Diastereopure Cobalt Catalysts Derived from Trications of the Formula [Co-(NH₂CHArCHArNH₂)₃]³⁺. *Inorg. Chem.* **2017**, *56*, 2304–2320. (b) Ehnbom, A.; Ghosh, S. K.; Lewis, K. G.; Gladysz, J. A. Octahedral Werner complexes with substituted ethylenediamine ligands: a stereochemical primer for a historic series of compounds now emerging as a modern family of catalysts. *Chem. Soc. Rev.* **2016**, *45*, 6799–6811.
- (4) (a) Ganzmann, C.; Gladysz, J. A. Phase Transfer of Enantiopure Werner Cations into Organic Solvents: An Overlooked Family of Chiral Hydrogen Bond Donors for Enantioselective Catalysis. Chem. -Eur. J. 2008, 14, 5397-5400. (b) Lewis, K. G.; Ghosh, S. K.; Bhuvanesh, N.; Gladysz, J. A. Cobalt(III) Werner Complexes with 1,2-Diphenylethylenediamine Ligands: Readily Available, Inexpensive, and Modular Chiral Hydrogen Bond Donor Catalysts for Enantioselective Organic Synthesis. ACS Cent. Sci. 2015, 1, 50-56. (c) Ghosh, S. K.; Ganzmann, C.; Bhuvanesh, N.; Gladysz, J. A. Werner Complexes with ω -Dimethylaminoalkyl Substituted Ethylenediamine Ligands: Bifunctional Hydrogen-Bond-Donor Catalysts for Highly Enantioselective Michael Additions. Angew. Chem., Int. Ed. **2016**, 55, 4356–4360. Werner-Komplexe mit ω -Dimethylaminoalkylsubstitutierten Ethylendiaminliganden: bifunktionale H-Brückendonor-Katalysatoren für hoch enantioselektive Michael-Additionen. Angew. Chem. 2016, 128, 4429-4433. (d) Kumar, A.; Ghosh, S. K.; Gladysz, J. A. Tris(1,2-diphenylethylenediamine)cobalt(III) Complexes: Chiral Hydrogen Bond Donor Catalysts for Enantioselective α-Aminations of 1,3-Dicarbonyl Compounds. Org. Lett. 2016, 18, 760-763. (e) Joshi, H.; Ghosh, S. K.; Gladysz, J. A. Enantioselective Additions of Stabilized Carbanions to Imines Generated from α-Amido Sulfones By Using Lipophilic Salts of Chiral Tris(1,2diphenylethylenediamine) Cobalt(III) Trications as Hydrogen Bond Donor Catalysts. Synthesis 2017, 49, 3905-3915. (f) Maximuck, W. J.; Gladysz, J. A. Lipophilic chiral cobalt(III) complexes of hexaamine ligands: Efficacies as enantioselective hydrogen bond donor catalysts. Molecular Catalysis 2019, 473, 110360. (g) Kabes, C. Q.; Maximuck, W. J.; Ghosh, S. K.; Kumar, A.; Bhuvanesh, N.; Gladysz, J. A. Chiral Tricationic tris(1,2-diphenylethylenediamine) Cobalt(III) Hydrogen Bond Donor Catalysts with Defined Carbon/Metal Configurations; Matched/Mismatched Effects upon Enantioselectivities with Enantiomeric Chiral Counter Anions. ACS Catal. 2020, 10, 3249-3263. (h) Maximuck, W. J.; Ganzmann, C.; Alvi, S.; Hooda, K. R.; Gladysz, J. A. Rendering Classical Hydrophilic Enantiopure Werner Salts $[M(en)_3]^{n+} nX^-$ Lipophilic (M/n = Cr/3, Co/3, Rh/3, Ir/3, Pt/4);New Chiral Hydrogen Bond Donor Catalysts and Enantioselectivities as a Function of Metal and Charge. Dalton Trans. 2020, 49, 3680-3691.
- (5) (a) Scherer, A.; Mukherjee, T.; Hampel, F.; Gladysz, J. A. Metal-Templated Hydrogen Bond Donors as "Organocatalysts" for Carbon-Carbon Bond Forming Reactions: Syntheses, Structures, and

- Reactivities of 2-Guanidinobenzimidazole Cyclopentadienyl Ruthenium Complexes. *Organometallics* **2014**, *33*, *6709–6722*. (b) Mukherjee, T.; Ganzmann, C.; Bhuvanesh, N.; Gladysz, J. A. Syntheses of Enantiopure Bifunctional 2-Guanidinobenzimidazole Cyclopentadienyl Ruthenium Complexes: Highly Enantioselective Organometallic Hydrogen Bond Donor Catalysts for Carbon-Carbon Bond Forming Reactions. *Organometallics* **2014**, *33*, *6723–6737*. (c) Mukherjee, T.; Ghosh, S. K.; Wititsuwannakul, T.; Bhuvanesh, N.; Gladysz, J. A. Chiral-at-Metal Ruthenium Complexes with Guanidinobenzimidazole and Pentaphenylcyclopentadienyl Ligands: Synthesis, Resolution, and Preliminary Screening as Enantioselective Second Coordination Sphere Hydrogen Bond Donor Catalysts. *Organometallics* **2020**, DOI: 10.1021/acs.organomet.0c00073.
- (6) Thomas, C.; Gladysz, J. A. Highly Active Families of Catalysts for the Ring-Opening Polymerization of Lactide: Metal Templated Organic Hydrogen Bond Donors Derived from 2-Guanidinobenzimidazole. ACS Catal. 2014, 4, 1134–1138.
- (7) (a) Chen, L.-A.; Tang, X.; Xi, J.; Xu, W.; Gong, L.; Meggers, E. Chiral-at-Metal Octahedral Iridium Catalyst for the Asymmetric Construction of an All-Carbon Quaternary Stereocenter. Angew. Chem., Int. Ed. 2013, 52, 14021-14025. Angew. Chem. 2013, 125, 14271-14275. (b) Chen, L.-A.; Xu, W.; Huang, B.; Ma, J.; Wang, L.; Xi, J.; Harms, K.; Gong, L.; Meggers, E. Asymmetric Catalysis with an Inert Chiral-at-Metal Iridium Complex. J. Am. Chem. Soc. 2013, 135, 10598-10601. (c) Xu, W.; Arieno, M.; Löw, H.; Huang, K.; Xie, X.; Cruchter, T.; Ma, Q.; Xi, J.; Huang, B.; Wiest, O.; Gong, L.; Meggers, E. Metal-Templated Design: Enantioselective Hydrogen-Bond-Driven Catalysis Requiring Only Parts-per-Million Catalyst Loading. J. Am. Chem. Soc. 2016, 138, 8774-8780. (d) Belokon, Y. N.; Maleev, V. I.; North, M.; Larionov, V. A.; Savel'yeva, T. F.; Nijland, A.; Nelyubina, Y. V. Chiral Octahedral Complexes of Co^{III} As a Family of Asymmetric Catalysts Operating under Phase Transfer Conditions. ACS Catal. 2013, 3, 1951-1955. (e) Maleev, V. I.; North, M.; Larionov, V. A.; Fedyanin, I. V.; Savel'yeva, T. F.; Moscalenko, M. A.; Smolyakov, A. F.; Belokon, Y. N. Chiral Octahedral Complexes of Cobalt(III) as "Organic Catalysts in Disguise" for the Asymmetric Addition of a Glycine Schiff Base Ester to Activated Olefins. Adv. Synth. Catal. 2014, 356, 1803-1810. (f) Ruley, Y. A.; Larionov, V. A.; Lokutova, A. V.; Moskalenko, M. A.; Lependina, O. L.; Maleev, V. I.; North, M.; Belokon, Y. N. Chiral Cobalt(III) Complexes as Bifunctional Brønsted Acid-Lewis Base Catalysts for the Preparation of Cyclic Organic Carbonates. ChemSusChem 2016, 9, 216-222. (g) Skubi, K. L.; Kidd, J. B.; Jung, H.; Guzei, I. A.; Baik, M.-H.; Yoon, T. P. Enantioselective Excited-State Photoreactions Controlled by a Chiral Hydrogen-Bonding Iridium Sensitizer. J. Am. Chem. Soc. 2017, 139, 17186-17192.
- (8) (a) Flock, A. M.; Krebs, A.; Bolm, C. Ephedrine- and Pseudoephedrine-Derived Thioureas in Asymmetric Michael Additions of Keto Esters and Diketones to Nitroalkenes. *Synlett* **2010**, 2010, 1219–1222. (b) Okino, T.; Hoashi, Y.; Furukawa, T.; Xu, X.; Takemoto, Y. Enantio- and Diastereoselective Michael Reaction of 1,3-Dicarbonyl Compounds to Nitroolefins Catalyzed by a Bifunctional Thiourea. *J. Am. Chem. Soc.* **2005**, 127, 119–125. (c) Nemoto, T.; Obuchi, K.; Tamura, S.; Fukuyama, T.; Hamada, Y. Novel chiral hydrogen bond donor catalysts based on a 4,5-diaminoxanthene scaffold: application to enantioselective conjugate addition of 1,3-dicarbonyl compounds to nitroalkenes. *Tetrahedron Lett.* **2011**, 52, 987–991.
- (9) The $^1\mathrm{H}$ and $^{13}\mathrm{C}$ NMR spectra agree well with those previously reported. 8
- (10) The dominant configuration was assigned by chiral HPLC using conditions similar to those in the literature.⁸
- (11) Frisch, M. J.; Trucks, G. W.; Schlegel, H. B.; Scuseria, G. E.; Robb, M. A.; Cheeseman, J. R.; Scalmani, G.; Barone, V.; Mennucci, B.; Petersson, G. A.; Nakatsuji, H.; Caricato, M.; Li, X.; Hratchian, H. P.; Izmaylov, A. F.; Bloino, J.; Zheng, G.; Sonnenberg, J. L.; Hada, M.; Ehara, M.; Toyota, K.; Fukuda, R.; Hasegawa, J.; Ishida, M.; Nakajima, T.; Honda, Y.; Kitao, O.; Nakai, H.; Vreven, T.; Montgomery, J. A., Jr.; Peralta, J. E.; Ogliaro, F.; Bearpark, M.;

- Heyd, J. J.; Brothers, E.; Kudin, K. N.; Staroverov, V. N.; Kobayashi, R.; Normand, J.; Raghavachari, K.; Rendell, A.; Burant, J. C.; Iyengar, S. S.; Tomasi, J.; Cossi, M.; Rega, N.; Millam, J. M.; Klene, M.; Knox, J. E.; Cross, J. B.; Bakken, V.; Adamo, C.; Jaramillo, J.; Gomperts, R.; Stratmann, R. E.; Yazyev, O.; Austin, A. J.; Cammi, R.; Pomelli, C.; Ochterski, J. W.; Martin, R. L.; Morokuma, K.; Zakrzewski, V. G.; Voth, G. A.; Salvador, P.; Dannenberg, J. J.; Dapprich, S.; Daniels, A. D.; Farkas, Ö.; Foresman, J. B.; Ortiz, J. V.; Cioslowski, J.; Fox, D. J. Gaussian 09, Rev, D.01; Gaussian, Inc.: Wallingford, CT, 2009.
- (12) (a) Grimme, S. Semiempirical GGA-Type Density Functional Constructed with a Long-Range Dispersion Correction. *J. Comput. Chem.* **2006**, 27, 1787–1799. (b) Chai, J.-D.; Head-Gordon, M. Long-range corrected hybrid density functionals with damped atomatom dispersion corrections. *Phys. Chem. Chem. Phys.* **2008**, 10, 6615–6620.
- (13) (a) Li, H.; Hall, M. B. Mechanism of the Formation of Carboxylate from Alcohols and Water Catalyzed by a Bipyridine-Based Ruthenium Complex: A Computational Study. *J. Am. Chem. Soc.* **2014**, *136*, 383–395. (b) Minenkov, Y.; Singstad, Å.; Occhipinti, G.; Jensen, V. R. The accuracy of DFT-optimized geometries of functional transition metal compounds: a validation study of catalysts for olefin metathesis and other reactions in the homogeneous phase. *Dalton Trans.* **2012**, *41*, 5526–5541.
- (14) Bergner, A.; Dolg, M.; Küchle, W.; Stoll, H.; Preuß, H. *Ab initio* energy-adjusted pseudopotentials for elements of groups 13–17. *Mol. Phys.* **1993**, *80*, 1431–1441.
- (15) (a) Hariharan, P. C.; Pople, J. A. The Influence of Polarization Functions on Molecular Orbital Hydrogenation Energies. *Theor. Chim. Acta* 1973, 28, 213–222. (b) Petersson, G. A.; Bennett, A.; Tensfeldt, T. G.; Al-Laham, M. A.; Shirley, W. A.; Mantzaris, J. A complete basis set model chemistry. I. The total energies of closed-shell atoms and hydrides of the first-row elements. *J. Chem. Phys.* 1988, 89, 2193–2218. (c) Petersson, G. A.; Al-Laham, M. A. A complete basis set model chemistry. II. Open-shell systems and the total energies of the first-row atoms. *J. Chem. Phys.* 1991, 94, 6081–6090.
- (16) Marenich, A. V.; Cramer, C. J.; Truhlar, D. G. Universal Solvation Model Based on Solute Electron Density and on a Continuum Model of the Solvent Defined by the Bulk Dielectric Constant and Atomic Surface Tensions. *J. Phys. Chem. B* **2009**, *113*, 6378–6396.
- (17) (a) Barone, V.; Cossi, M. Quantum Calculation of Molecular Energies and Energy Gradients in Solution by a Conductor Solvent Model. *J. Phys. Chem. A* **1998**, *102*, 1995–2001. (b) Cossi, M.; Rega, N.; Scalmani, G.; Barone, V. Energies, Structures, and Electronic Properties of Molecules in Solution with the C-PCM Solvation Model. *J. Comput. Chem.* **2003**, *24*, 669–681.
- (18) Cramer, C. J. Essentials of Computational Chemistry: Theories and Models, 2nd ed.; Wiley: Chichester, United Kingdom, 2006; Chapter 10.5.4.
- (19) (a) Schäfer, A.; Horn, H.; Ahlrichs, R. Fully optimized contracted Gaussian basis sets for atoms Li to Kr. *J. Chem. Phys.* **1992**, 97, 2571–2577. (b) Schäfer, A.; Huber, C.; Ahlrichs, R. Fully optimized contracted Gaussian basis sets of triple zeta valence quality for atoms Li to Kr. *J. Chem. Phys.* **1994**, 100, 5829–5835.
- (20) Ribeiro, R. F.; Marenich, A. V.; Cramer, C. J.; Truhlar, D. G. Use of Solution-Phase Vibrational Frequencies in Continuum Models for the Free Energy of Solvation. *J. Phys. Chem. B* **2011**, *115*, 14556–14562.
- (21) (a) Hall, M. B.; Fenske, R. F. Electronic Structure and Bonding in Methyl- and Perfluoromethyl(pentacarbonyl)manganese. *Inorg. Chem.* **1972**, *11*, 768–775. (b) Webster, C. E.; Pérez, L. M.; Hall, M. B. http://www.chem.tamu.edu/jimp2/index.html (accessed August 2019). (c) Bursten, B. E.; Jensen, J. R.; Fenske, R. F. An Χα optimized atomic orbital basis. *J. Chem. Phys.* **1978**, *68*, 3320–3321.
- (22) Wititsuwannakul, T.; Hall, M. B.; Gladysz, J. A. A Computational Study of Hydrogen Bonding Motifs in Halide, Tetrafluoroborate, Hexafluorophosphate, and Tetraarylborate Salts of Cationic Ruthenium and Cobalt Guanidinobenzimidazole Hydrogen Bond

- Donor Catalysts; Acceptor Properties of the "BAr $_{\rm f}$ " Anion. *Polyhedron* 2020, in press.
- (23) Mills, S. G.; Beak, P. Solvent Effects on Keto-Enol Equilibria: Tests of Quantitative Models. *J. Org. Chem.* **1985**, *50*, 1216–1224.
- (24) It is worth keeping in mind that the cyclic enol of 2,4-pentanedione exhibits a "double potential energy minimum", i.e. the O=H bonds are not of equal length: Emsley, J.; Ma, L. Y. Y.; Bates, P. A.; Motevalli, M.; Hursthouse, M. B. β -Diketone Interactions Part 8. The Hydrogen Bonding of the Enol Tautomers of Some 3-Substituted Pentane-2,4-diones. *J. Chem. Soc., Perkin Trans.* 2 **1989**, 527–533.
- (25) Plata, R. E.; Singleton, D. A. A Case Study of the Mechanism of Alcohol-Mediated Morita Baylis-Hillman Reactions. The Importance of Experimental Observations. *J. Am. Chem. Soc.* **2015**, *137*, 3811–3826
- (26) Takemoto, Y. Development of Chiral Thiourea Catalysts and Its Application to Asymmetric Catalytic Reactions. *Chem. Pharm. Bull.* **2010**, *58*, 593–601.
- (27) Hamza, A.; Schubert, G.; Soós, T.; Pápai, I. Theoretical Studies on the Bifunctionality of Chiral Thiourea-Based Organocatalysts: Competing Routes to C-C Bond Formation. *J. Am. Chem. Soc.* **2006**, 128, 13151–13160.
- (28) Ayala, P. Y.; Schlegel, H. B. Identification and treatment of internal rotation in normal mode vibrational analysis. *J. Chem. Phys.* **1998**, *108*, 2314–2325.
- (29) Technically, the energy differences between the isomers in Figure 13 should be compared to the difference in *electronic* energies of $TS_{CC}9'$ and $TS_{CC}12$ -I (3.3 kcal/mol; Table s18 in the Supporting Information) as opposed to free energies (2.6 kcal/mol).
- (30) (a) Chen, D.; Lu, N.; Zhang, G.; Mi, S. The mechanism of enantioselective control of an organocatalyst with central and axial chiral elements. *Tetrahedron: Asymmetry* **2009**, *20*, 1365–1368. (b) Zhu, J.-L.; Zhang, Y.; Liu, C.; Zheng, A.-M.; Wang, W. Insights into the Dual Activation Mechanism Involving Bifunctional Cinchona Alkaloid Thiourea Organocatalysts: An NMR and DFT Study. *J. Org. Chem.* **2012**, *77*, 9813–9825.
- (31) Varga, S.; Jakab, G.; Drahos, L.; Holczbauer, T.; Czugler, M.; Soós, T. Double Diastereocontrol in Bifunctional Thiourea Organocatalysis: Iterative Michael-Michael-Henry Sequence Regulated by the Configuration of Chiral Catalysts. *Org. Lett.* **2011**, *13*, 5416–5419.
- (32) (a) Yang, C.; Wang, J.; Liu, Y.; Ni, X.; Li, X.; Cheng, J.-P. Study on the Catalytic Behavior of Bifunctional Hydrogen-Bonding Catalysts Guided by Free Energy Relationship Analysis of Steric Parameters. *Chem. Eur. J.* **2017**, 23, 5488–5497. (b) Jiménez, E. I.; Vallejo Narváez, W. E.; Román-Chavarría, C. A.; Vazquez-Chavez, J.; Rocha-Rinza, T.; Hernández-Rodríguez, M. Bifunctional Thioureas with α-Trifluoromethyl or Methyl Groups: Comparison of Catalytic Performance in Michael Additions. *J. Org. Chem.* **2016**, 81, 7419–7431.
- (33) (a) Grayson, M. N.; Houk, K. N. Cinchona Urea-Catalyzed Asymmetric Sulfa-Michael Reactions: The Brønsted Acid-Hydrogen Bonding Model. *J. Am. Chem. Soc.* **2016**, 138, 9041–9044. (b) Grayson, M. N.; Houk, K. N. Cinchona Alkaloid-Catalyzed Asymmetric Conjugate Additions: The Bifunctional Brønsted Acid-Hydrogen Bonding Model. *J. Am. Chem. Soc.* **2016**, 138, 1170–1173. (c) Grayson, M. N. Mechanism and Origins of Stereoselectivity in the Cinchona Thiourea- and Squaramide-Catalyzed Asymmetric Michael Addition of Nitroalkanes to Enones. *J. Org. Chem.* **2017**, 82, 4396–4401.